Title	FAR-INFRARED PHOTOCONDUCTIVITY IN GALLIUM ARSENIDE
Author(s)	宮尾, 正信
Citation	大阪大学, 1974, 博士論文
Version Type	VoR
URL	https://hdl.handle.net/11094/422
rights	
Note	

FAR-INFRARED PHOTOCONDUCTIVITY
IN
GALLIUM ARSENIDE

MASANOBU MIYAO

MARCH 1974

Acknowledgements

This research was suggested by Professor S.Narita and has been investigated under his careful guidance and encouragement. This is greatly acknowledged.

I would also like to thank Dr.Y.Nisida and other members of our laboratory for their helpful suggestions and useful discussions.

Special thanks are extended to Dr.H.Harada of the Nippon Telegraph and Telephone Public Corp., and also to Dr.O.Ryuzan of the Fujitsu Laboratories for providing us with samples.

Abstract

(I) Magnetic field dependences of the far-infrared photoconductivity spectra of GaAs with donor concentrations of $4.7\times10^{14}\sim2.0\times10^{15}\mathrm{cm}^{-3}$ have been investigated at 4.2K. For low impurity concentration cases, we have six spectral peaks at a magnetic field in the photoconductivity spectra due to the electron transitions from the ground state to the excited states of the shallow impurity center. It is found from the comparison of the experimental results with the calculations by the variation method that the electronic states of the shallow donors in an usual magnetic field range can be precisely expressed by harmonic oscillator wave functions rather than hydrogen-like ones.

Donor concentration- and magnetic field-dependences of the spectral line widths in a magnetic field are studied and the broadening effects are attributed to the increasing of the interactions between the neighboured donors with increasing donor concentrations or with decreasing magnetic field.

(II) In order to investigate the far-infrared photoconductivity mechanism in impurity doped GaAs, we measured the impurity concentration dependent photoconductive response as a function of temperature, and we also measured the Hall coefficient and resistivity vs temperature curves in various impurity concentrations for comparison. For the explanation of the experimental results of the photoconductivity, the cascade capture theory and its modified forms are used.

In a low impurity concentration case, photoconductive responses associated with the transitions from the ground state to the conduction band and those with the transitions from the ground state to the 2p

excited state are qualitatively explained by the cascade capture model. The mechanism of the photoconductivity associated with the 2p excited state is believed to be photo-thermal ionization. The smallness of the apparent activation energy of the electron in the 2p state experimentally obtained is well interpreted by the cascade capture model.

In a high impurity concentration case, the experimental results of the photoconductivity vs inverse temperature curves are appreciably deviated from the calculated ones by the normal cascade capture model. It is supposed that the above discrepancy is originated in the changes of the excited levels with increasing impurity concentration. We propose a modification of the cascade capture model, in which the role of the high excited states transfering the electrons from the lower states to the conduction band is reduced with increasing donor concentration. We also introduce for highly doped samples an impurity conduction through the 2p excited states to explain the invariant of the number of the photoconductive carrier with temperature in the low temperature region.

CONTENTS

§1. Introduction

Most of the investigations on the impurity states in Ge[1] and Si[2] have been done by means of the galvanomagnetic effects in wide temperature ranges, and several impurity concentration effect have been observed. The impurity conduction or conduction in the impurity band is believed to occure in considerably low temperature region for heavily doped semiconductors, though many problems have remained unsolved for the intermediately doped samples. The progress in the techniques of high quality sample preparations for InSb have brought many interesting reports on the galvanomagnetic effects of this material.
At present, we have many data of the magnetic field and electric field effect on the material containing the magnetically induced Mott transition effect[3] and the strong non-Ohmic properties[4] due to the hot electron.

On the other hand, the far-infrared investigations for these materials have become active in these ten years, and many new information on the excited states of impurity centers in the semiconductors have been added to our knowledges. One of the main subjects in the study of the far-infrared absorption spectra for Ge,[5,6,7] Si[8] and InSb[9] is the energy states of the localized shallow donors, and especially the effect of the magnetic field on the energies in the low impurity concentration case. Another subject is concerned with the variation of the absorption spectra with increasing impurity concentration, being related to the impurity conduction. The far-infrared photoconductivity in Ge[10,11] and InSb[12,13] have been also measured. The photoconductivity measurements can be also considered as one of the most powerful tools for the study on the impurity states of the semiconductors and this phenomena have been practically utilized as far-infrared detectors.

We have known from the theoretical and experimental investigations on the impueiry states in Ge and Si that the electronic levels of the shallow donors can be expressed by the hydrogenic model for low impurity concentration samples, and this model becomes invalid being due to the interactions between the neighboured donors with increasing donor concentrations. In the case of Ge and Si, their complex energy bands make difficult the comparisons between the experimental results and the theory. While in the case of InSb, the overlappings of the wave functions due to the large Bohr radius of the material prevent us to measure the isolated properties of the donors.

Recently the techniques for the crystal-growth of GaAs,14) have considerably advanced by the method of the so-called "epitaxial growth" and it has enabled us to carry out the study on the donor states of GaAs. Fortunately, the conduction band has its minimum at zero-wave vector, that is, the band is isotropic around the minimum and in addition to it, the effective mass has an appropriate value for many studies. Measurements of the galvanomagnetic effects in GaAs15,16) have been carried out, and various properties associated with the impurity states, such as the non-metal to metal transition of the conductivity, the conduction in a high magnetic field, and the non-Ohmic behavior due to the hot electron, are observed simultaneously by the use of the single material GaAs. Far-infrared photoconductivity measurements for GaAs17∿22) have been mainly performed for the specimens with low impurity concentrations. The main purpose of the measurements was the study on the energy states of the isolated donors in GaAs and the developement of far-infrared photoconductivity detectors with high sensitivity and short response time.

The investigation of the impurity concentration dependence of photoconductivity is very interesting not only from the view point of solid state physics, but also from the point of detector technology. That is, physicists have interested in the changes of the energy states of impurity centers with increasing donor concentrations and technologysts have looked for the optimum condition of the donor concentration for the photoconductive response. Though we have many reports on the impurity concentration dependence of galvanomagnetic effects in GaAs, only two reports 23,24) were concerned with the impurity concentration effects on photoconductivities and optical absorption coefficients. Moreover, even in the papers, they reported only about the fact that the line width associated with the electron transitions from the ground state to the first excited state of impurity center becomes broader and the photoconductive response becomes smaller with increasing donor concentrations.

The present paper can be divided into two subjects; one of them is the study of the effects of the magnetic field on the localized energy levels in GaAs by means of far-infrared photoconductivity techniques and the experimental results are compared with the theoretically expected levels calculated by the variation method. The other one is the study of the effects of the impurity concentration on the photoconductivity. The measurements of the photoconductivity are performed as a function of temperature and the mechanism of the photoconductivity change with impurity concentration will be discussed.

§2. Experimental procedures

The samples used in the present experiment were grown by vapor phase epitaxy on Cr-doped semi-insulating GaAs crystals having (100) oriented surface. The physical properties are listed in Table 1. Electrical contacts to the samples were made by alloying pure tin to the epitaxial layers at about 350°C in reducing atomosphere.

The experimental arrangements shown in Figs.1 and 2 were prepared for the electrical measurements and also used for the photoconductivity measurements. In all the measurements for temperatures between 4.2K and 1.6K, the samples were immersed in liquid helium and for temperatures above 4.2K, the sample chamber was kept in vacuum, and the temperature was increased by manganin heater. The temperature were estimated by measuring the change of the resistivity of a germanium probe having donor concentration of $9\times10^{14}\text{cm}^{-3}$ 1) in a dark condition.

The resistivity, ρ, and the Hall coefficient, R_H, of the sample were measured by van der Paw's method 25) in a dark condition. While the compensation ratios of the samples were calculated by applying the Brooks-Herring formula to the relation between the mobility and carrier concentration at 77K and 300K.26)

In the photoconductivity measurement, the electrical current was flown to the specimen using a constant current circuit and the signal voltage between the electrodes, which were contacted to the both sides of the sample, was amplified by high input impedance amplifier shown in Fig.3.

The instrument employed was a Hitachi model FIS-21 far-infrared spectrometer, and the monochromatic light from the spectrometer was introduced into a light pipe. A superconducting magnet of Nb-Zr was used for the measurements in a magnetic field. In the photoconductivity measurements, the sample position relative to the magnetic field in the light pipe was varied so that the relative angle between the electric field vector $\vec{E}$ of the incident light and the magnetic field vector $\vec{H}$ could be changed. The configuration in which the sample surface is perpendicular to $\vec{H}$ will be called "nearly Faraday configuration" and that in which the surface is parallel to $\vec{H}$ "nearly Voigt configuration". The reason for calling "nearly" is that in the light pipe system a mixing of the components of $\vec{E}$ perpendicular and parallel to $\vec{H}$ is unavoidable.

Table 1. Galvanomagnetic properties of GaAs samples used.

sample name	N_D cm^{-3}	compensation ratio N_A/N_D	mobility at 77K $\mathrm{cm}^2/\mathrm{V\cdot sec}$	analysis using 2 carrier model		
				μ_c $\mathrm{cm}^2/\mathrm{V\ sec}$	μ_i $\mathrm{cm}^2/\mathrm{V\cdot sec}$	T* K
TU4714	4.7×10^{14}	0.51	1.10×10^5			
TU6114	6.1×10^{14}	0.66	8.86×10^4	1.2×10^4	1.9	4.5
FU1215	1.2×10^{15}	0.50	6.72×10^4	8.5×10^3	3.3	5.1
FU2015	2.0×10^{15}	0.60	4.49×10^4	4.8×10^3	20	6.5
TU3015	3.0×10^{15}	0.37	4.33×10^4			

μ_c and μ_i are the electron mobility in the conduction band and the impurity state at T=T*. (T* are the temperatures at which the Hall coefficients have their maximum values.)

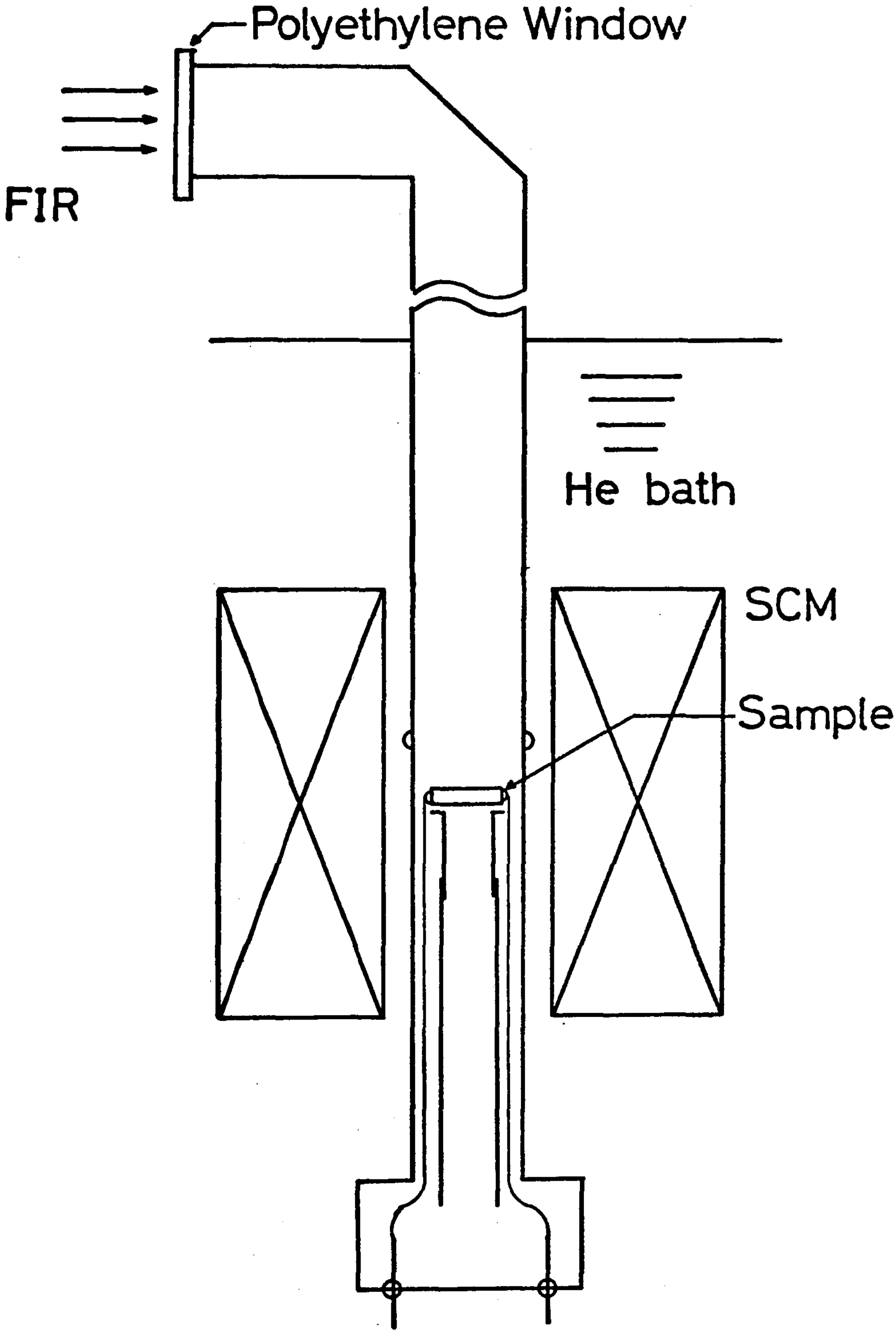

Fig.1. Experimental arrangement around sample for far-infrared photoconductivity measurements (in nearly Faraday configuration)

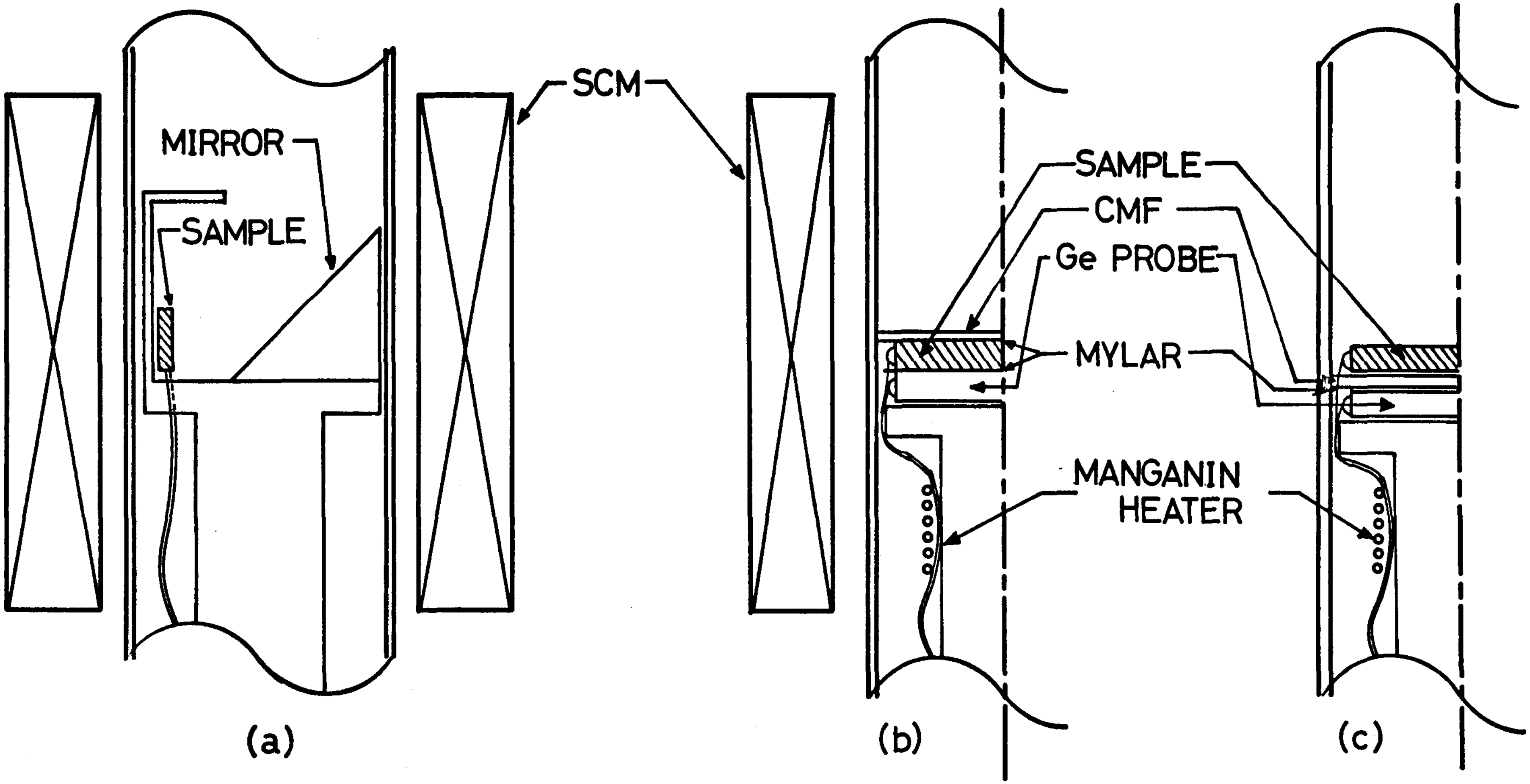

Fig.2. Details of the sample chambers; (a) used for the photoconductivity measurements in nearly Voigt configuration, (b) used for the measurements of Hall coefficient and resistivity, (c) used for the photoconductivity measurements above 4.2K. CMF; cold metal filter

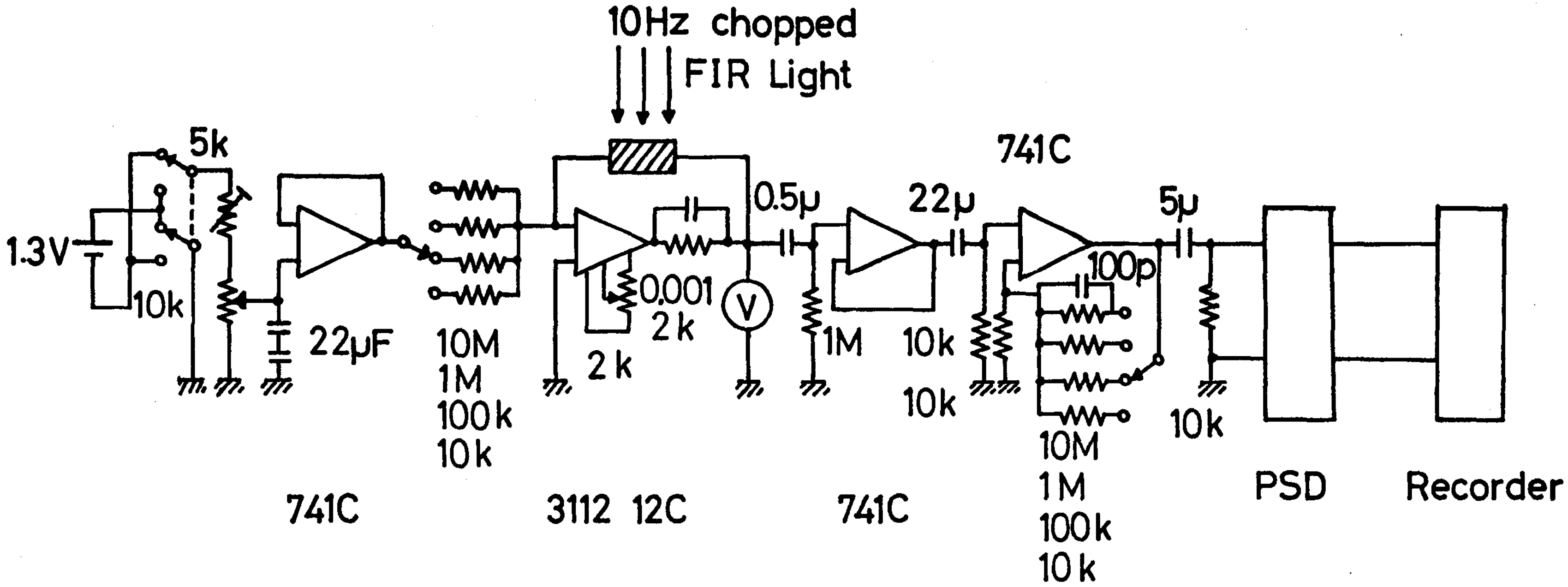

Fig.3. Diagram of the electronics for the measurements.

§3. Magnetic field effects on shallow donor states

3-1. Preliminaries

The problems of impurity states in semiconductors in magnetic fields have been studied by a number of investigators. One of their interests is the magnetic field dependences of the energy levels of impurity centers. Generally relative magnetic field intensity is represented by a parameter γ,[27] which is the ratio of the zero point energy of the lowest Landau level $\hbar\omega_c/2$ to the Coulomb binding energy R_y^*, that is;

$$\gamma=\hbar\omega_c/2R_y^* \ . \qquad (3.1.1)$$

In a magnetic field, a donor electron receives two main interactions, the Coulomb force due to the positively charged ion, and the force due to the applied magnetic field. In low field cases, $\gamma<<1$, the magnetic interaction can be recognized as a small perturbation so that usual hydrogenic Zeeman effect is observed and the electronic state of the impurity center is characterized by the symbols ($n\ell m$), where n is the principal quantum number, ℓ the quantum number for the orbital momentum, and m the quantum number for the angular momentum. In high field cases, $\gamma>>1$, the Coulomb interaction becomes a small perturbation, so that the behaviour of a donor electron resembles to a free carrier in a magnetic field and the electronic state of impurity center is characterized by ($NM\lambda$), where N is the principal quantum number, M the quantum number for the angular momentum about the magnetic field, and λ designates the bound Coulomb states.

Kleiner[28] and Elliot-Loudon[29] predicted the relations between ($n\ell m$) state and ($NM\lambda$) state using the concept of *nordal surface conservation.*

These relations are

$$m = M,$$
$$n-\ell-1= N-1/2\ (M+|M|), \qquad (3.1.2)$$
$$\ell-|m| = \lambda.$$

The transition from the low field approximation, (hydrogenic model), to the strong field approximation, (harmonic oscillator model), occurs in the intermediate field, $\gamma \simeq 1$. Therefore, the investigation in the intermediate region is very interesting.

Far-infrared magneto-optical investigations for InSb and Ge have been performed. In experiments of InSb[9,12,13] three peaks which correspond to the transitions from (000) to $(0\bar{1}0)$, (001) and (110) in the symbol $(NM\lambda)$ were observed. However these experiments were carried out in so high field range of 10∿100kOe which correspond to γ of 7∿70 that these results correspond only to the case of the high field limit. At fields much less than 10kOe and in currently available samples, the donor electron is no longer localized electron in a impurity state.

In the case of Ge,[7,13] the experiments were carried out in the field range of 0∿50kOe which correspond to γ of 0∿0.8 and the theoretical analysis were also performed using the variation method. However, the complications due to the many valley of the conduction band and the necessity of the central cell corrections for the ground state occured in the comparison between the experimental results and theoretical ones.

Recently crystal-growth technics for GaAs[14] have advanced and it has enabled us to carry out the far-infrared photoconductivity measurements of high purity epitaxial growth GaAs. The study of the donor state in GaAs can be done in the low and intermediate field region and moreover, this material has conduction band of single valley. Therefore GaAs is considered as one of the most ideal materials to investigate donor states in a magnetic field.

Magneto-optical spectra in high purity GaAs crystals have been observed by Kaplan et al.18) and Stillman et al.19) independently. Kaplan et al. have measured the photoconductivity spectra with samples of donor concentrations $1\sim7\times10^{14}cm^{-3}$ in magnetic fields up to 50kOe. They assigned to the four remarkable peaks in their spectra the transitions from the ground state (000) to the excited state $(0\bar{1}0)$, (001), (110) and (210) in the symbol (NMλ). They have considered 2p(m=-1), 2p(m=0), 2p(m=+1) and 3p(m=+1) correspond to $(0\bar{1}0)$, (001), (110) and (210) respectively by using the relations (3.1.2). Besides they calculated the energies of (000), $(0\bar{1}0)$, and (110) in magnetic fields with the hydrogenic effective mass theory and found a good agreement between their experimental curves and the theoretical ones.

Stillman et al. have made measurements of the far-infrared photoconductivity spectra using purer epitaxial GaAs crystals (the donor concentration=$4.8\times10^{13}cm^{-3}$) than those of Kaplan et al. in magnetic field up to 29.9kOe and they observed six distinguished peaks. They assigned to these peaks, successively from the lowest energy, the transitions from the ground state 1s to the excited hydrogenic donor states 2p(m=-1), 2p(m=0), 2p(m=+1), 3p(m=-1), 3p(m=0), and 3p(m=+1). Furthermore, they performed variational calculations for 1s and 2p(m=±1) using the trial functions given by Larsen31) and confirmed a good agreement between the theory and the experimental results.

3-2. Photoconductivity spectra in a magnetic field

In order to study magnetic field dependence of the donor levels and to examine the selection rules, far-infrared photoconductivity for the high purity specimen (TU4714) in a magnetic field for "nearly Faraday and Voigt configuration" has been carried out. The spectral responce of the photoconductivity at 4.2K per unit incident power in "nearly Faraday configuration" is shown in Figs.4, 5, and 6 for magnetic fields of 0, 12.5 and 27.6kOe respectively.

In a zero magnetic field a sharp peak at $35.5\mathrm{cm}^{-1}$, a weaker band over the shorter wavelength side, and a sharp decay of the response towards the longer wave length side are observed. In an applied magnetic field the sharp peak in zero field splits into a triplet and other peaks are observed. These results indicate that these peaks are due to transitions between the ground state and the excited states of a shallow donor levels in GaAs. The photoconductivity frequencies as functions of magnetic field are plotted by circles in Fig.7. In the same figure, a part of the results obtained by Kaplan et al.[18)] (squares) and those by Stillman et al.[19)] (triangles) are plotted for comparison. The three sets of data obtained independently are seen to be in good accord within experimental errors. To examine the selection rules $\Delta m=\pm1$, or 0, the results of the photoconductivity measurements in nearly Faraday configuration were compared with those in nearly Voigt configuration. Fig.8 shows the spectra at 12.5kOe, where peaks A and B correspond to the first and second lines from the bottom in Fig.7, and C and D to the highest two lines in the figure. The photoresponses are normalized at the A and D peaks respectively. The hight of the B peak assigned as $1s\rightarrow2p(m=0)$ by Stillman et al. or $(000)\rightarrow(001)$ by Kaplan et al. differs in the two configurations by a

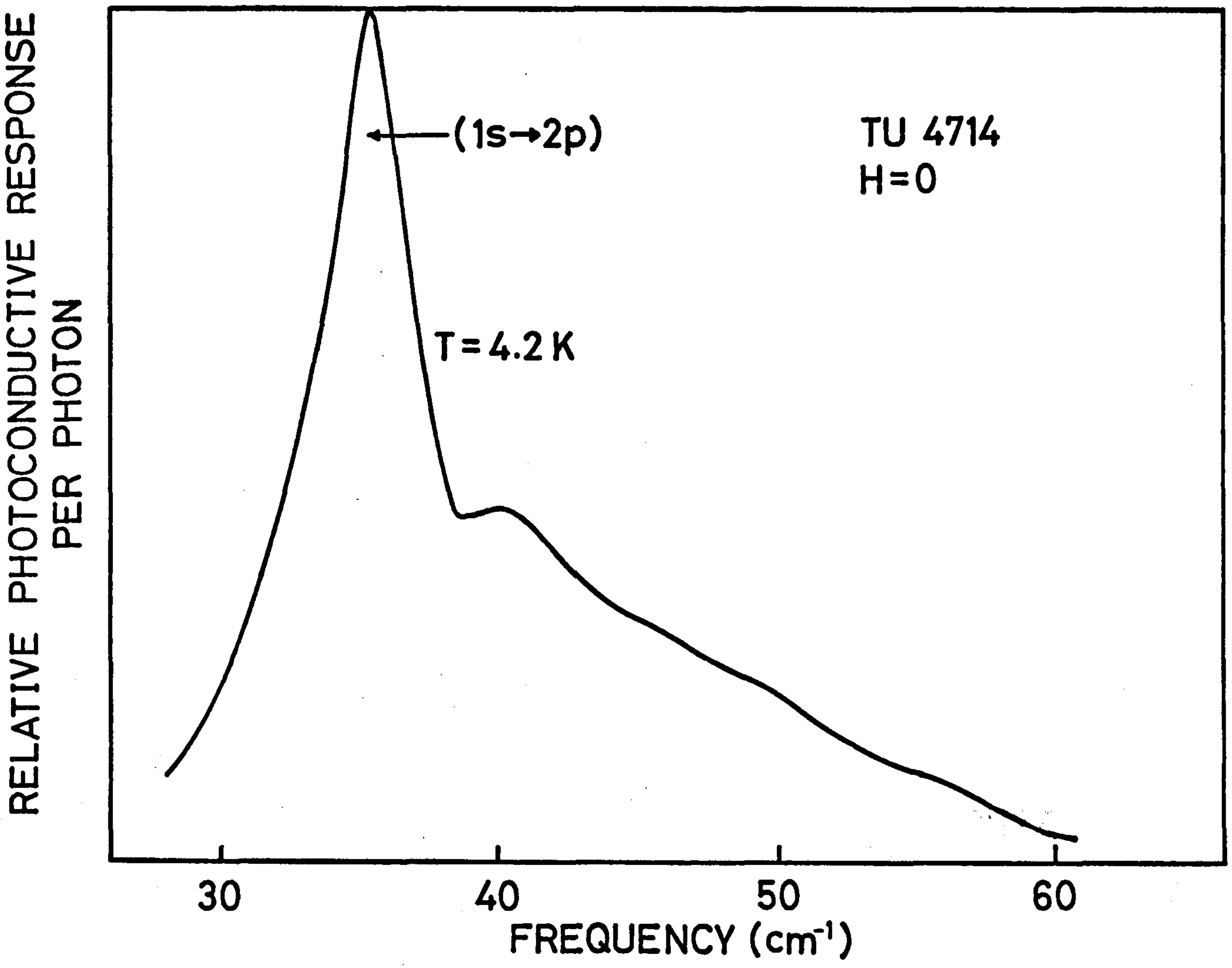

Fig.4. Spectral response of the photoconductivity at 4.2K without magnetic field for the sample of TU4714.

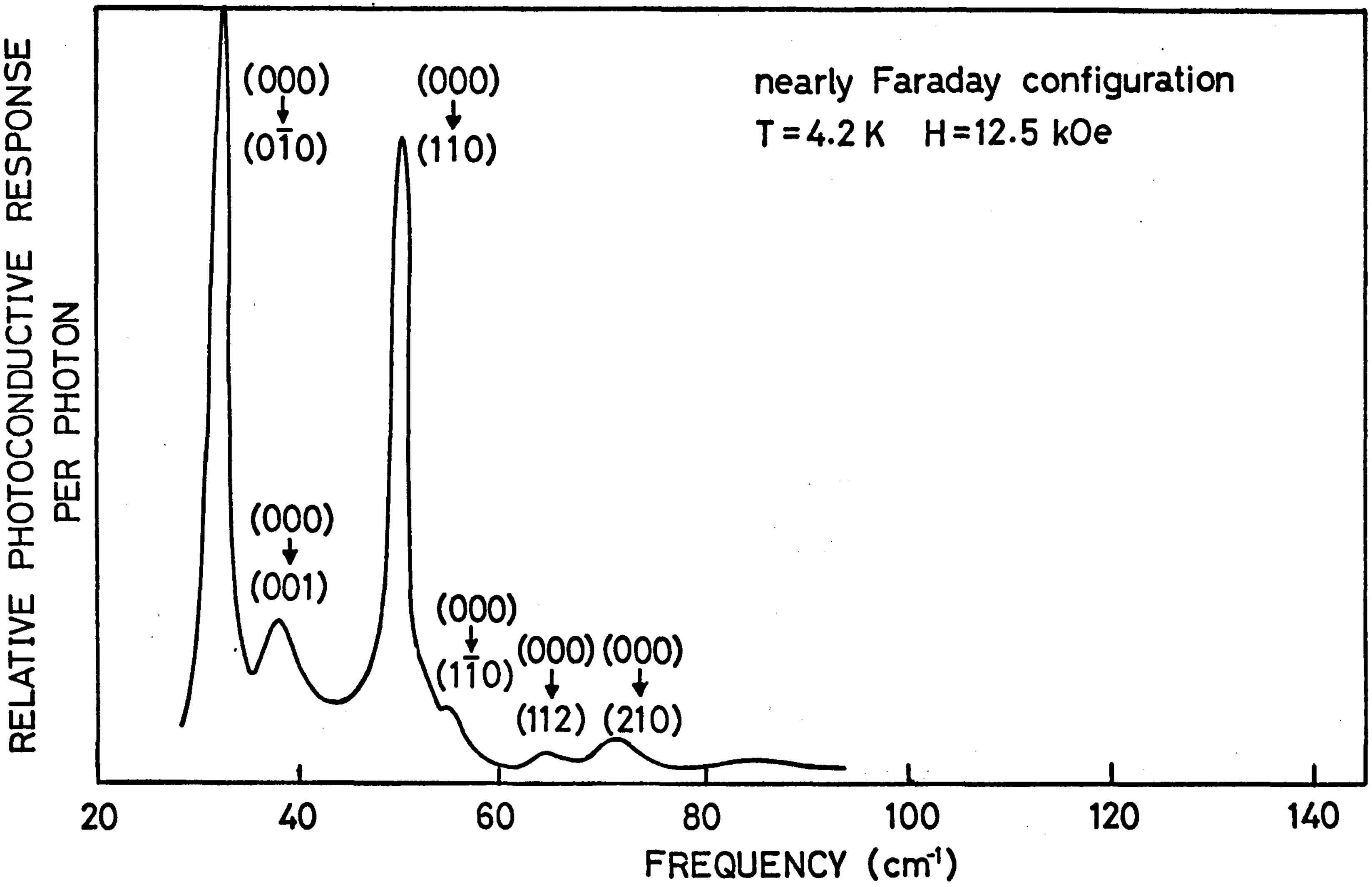

Fig.5. Spectral response of the photoconductivity at 4.2K with the magnetic field of 12.5kOe in nearly Faraday configuration for the sample of TU4714.

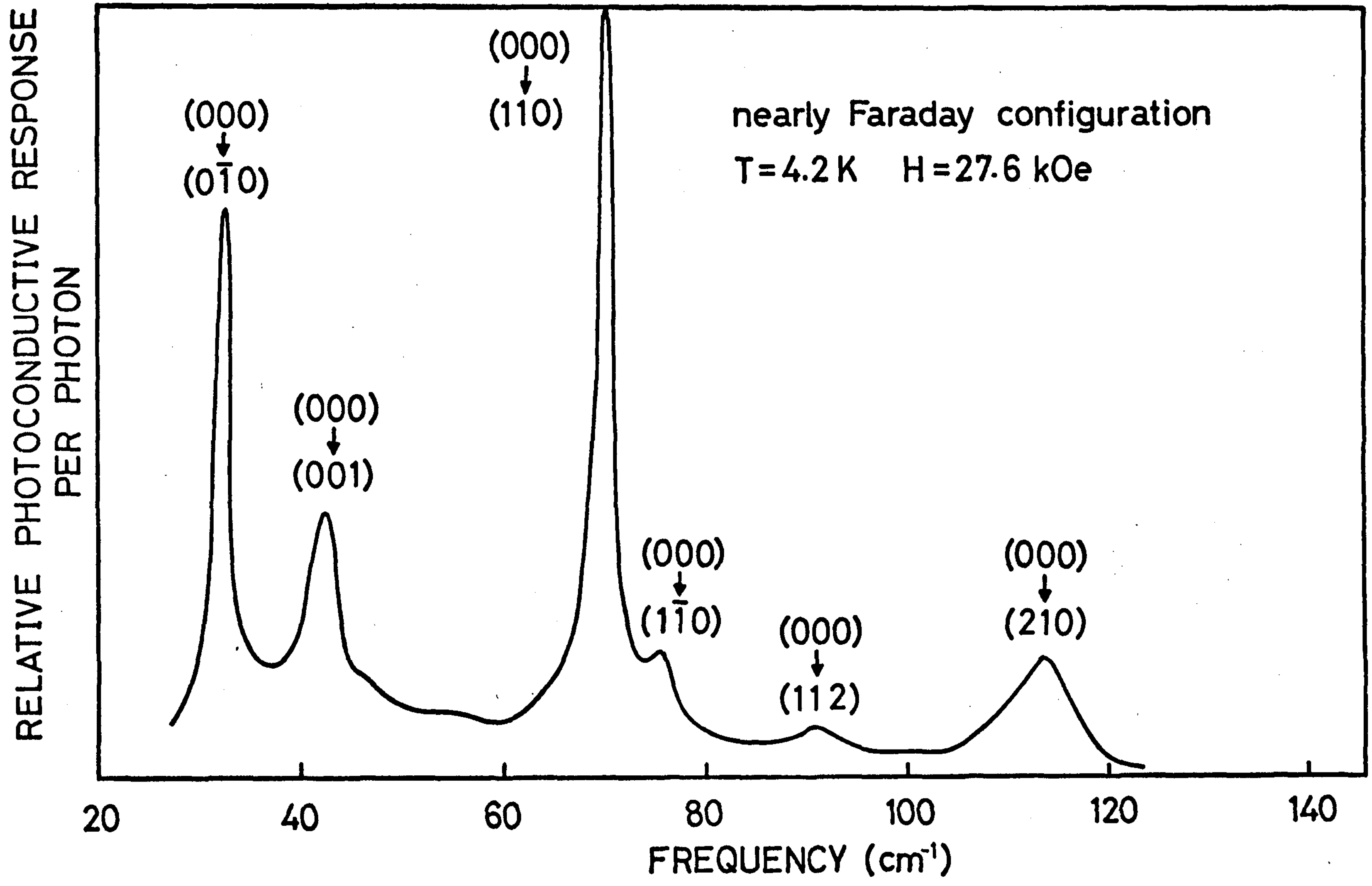

Fig.6. Spectral response of the photoconductivity at 4.2K with the magnetic field of 27.6kOe in nearly Faraday configuration for the sample of TU4714.

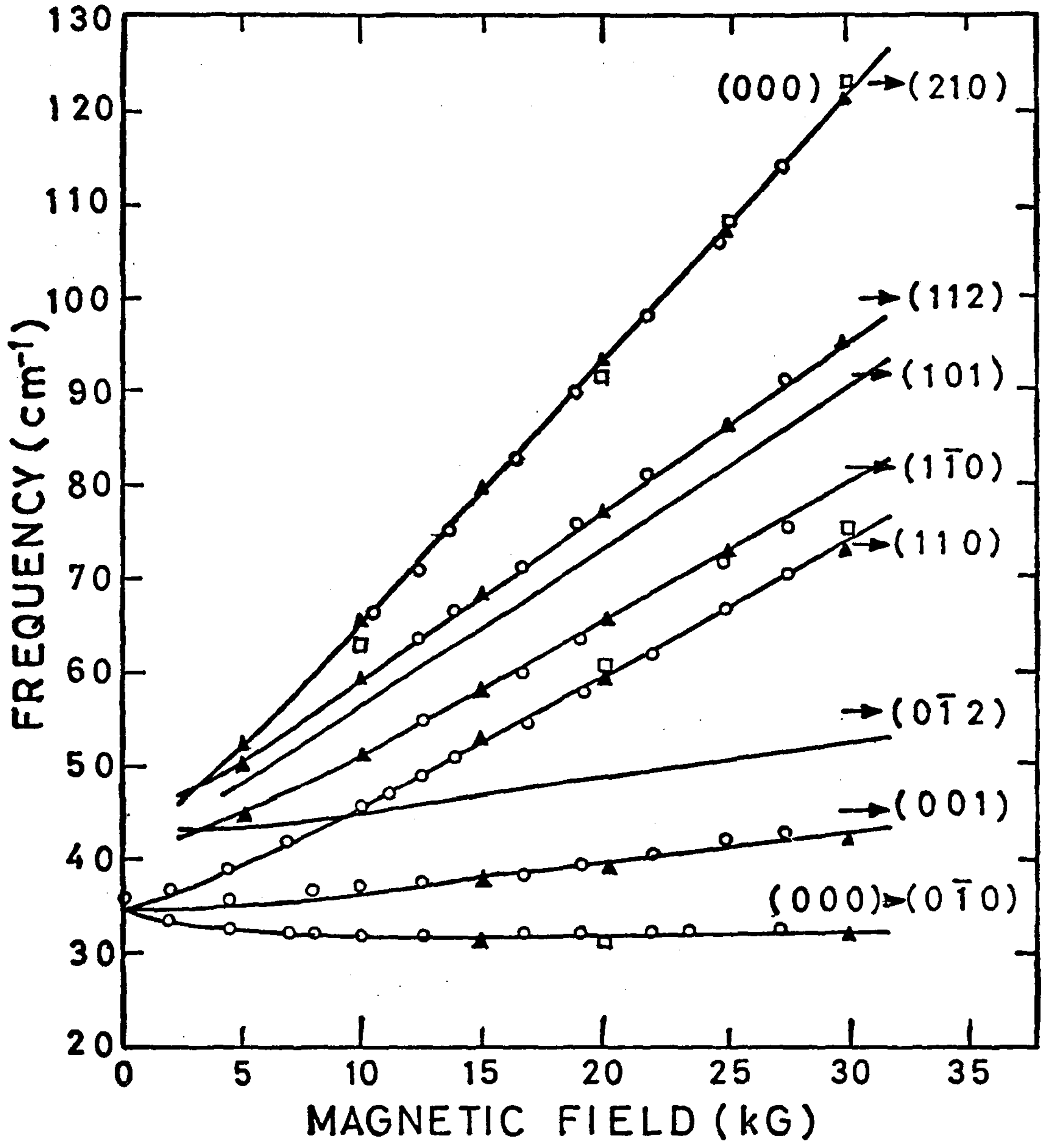

Fig.7. Experimental and theoretical transition energies as functions of magnetic field. Solid curves are from variational calculations and circles are experimental points. Part of the experimental results obtained by Kaplan et al.[18] (squares) and by Stillman et al.[19] (triangles) are also shown.

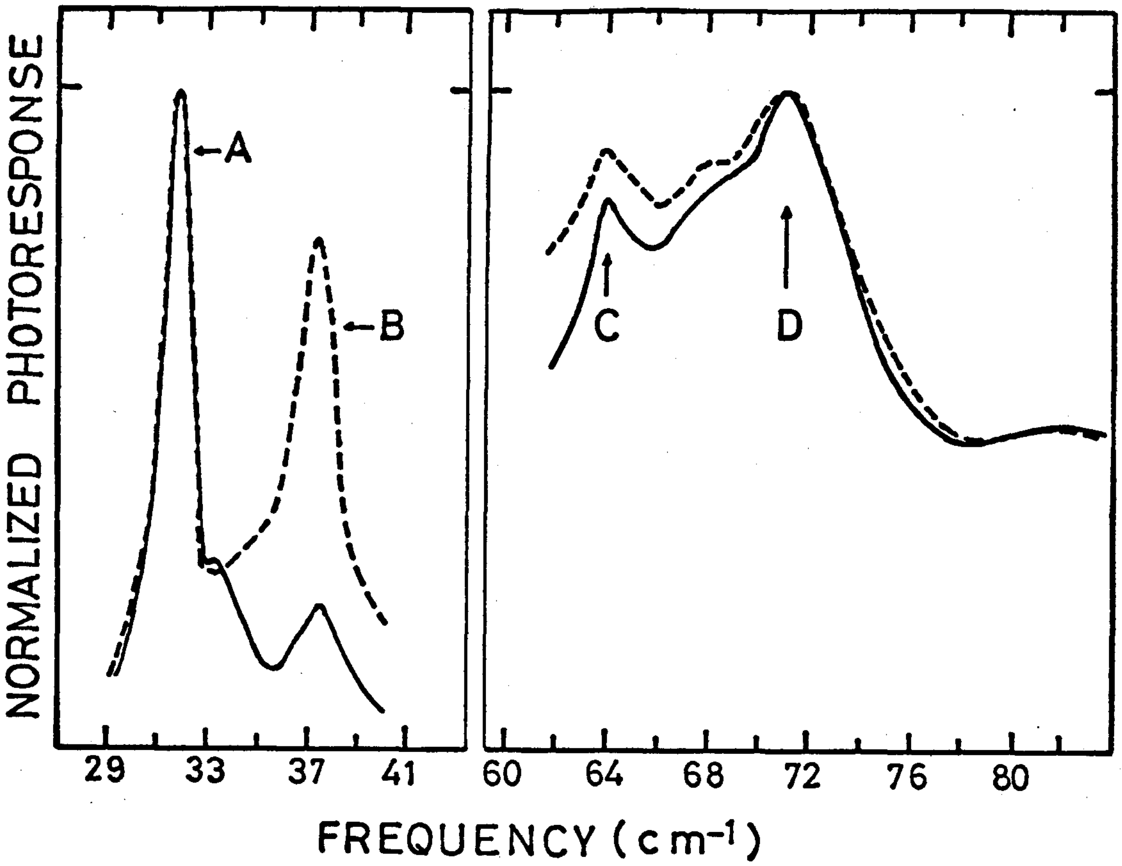

Fig.8. Photoconductivity excitation spectra in the energy range of 29∿41 cm^{-1} and 60∿84cm^{-1} in nearly Faraday configuration (solid curves) and in nearly Voigt configuration (broken curves) at 12.5kOe. The peaks A,B,C, and D have been assigned hitherto as the transition 1s→2p(m=-1), 1s→2p(m=0), 1s→3p(m=0), and 1s→3p(m=+1). The photoresponses are normalized at the A and D peaks, the real response at the A peak being about 14 times as large as that at the D peak.

factor of five, which indicates that this peak corresponds to a transition with $\Delta m=0$. On the other hand, the C peak assigned as $1s\rightarrow 3p(m=0)$ by Stillman et al. changes at most by 10 % between the two configurations, showing that this peak hardly corresponds to a transition with $\Delta m=0$.

Donor concentration dependence of photoconductivity spectra in a magnetic field is also observed. Fig.9 shows the normalized photoconductivity spectra in nearly Faraday configuration for specimens, TU6114, FU1215, and FU2015 at 4.2K and at 27.6kOe. These peaks correspond to the transition from (000) to (110) in the $(NM\lambda)$ symbol. Though the line width of the photoconductivity curve broadens, the position of the maximum response of the line does not shift with increasing donor concentration.

Fig.10 shows the magnetic field dependences of the line width of the various peak lines for the high purity specimen TU6114. All line widths become narrow with increasing magnetic field and converge to a constant value (about $1.3cm^{-1}$) above 15kOe. Besides $(000)\rightarrow(001)$ line width is slightly broader than $(000)\rightarrow(110)$ and $(000)\rightarrow(0\bar{1}0)$ line widths. However the spectral line widths above 15kOe are limited by the resolution of the spectrometer. In a similar experiment by Stillman et al.22) by the use of Fourier spectrometer with a resolution of $0.076cm^{-1}$, they indicate that each transition peak can be separated to three peaks. This results mean that three different residual and unidentified donor impurities in epitaxial GaAs realize the slightly different energy position of the ground states due to the central cell corrections. In the experiment shown in Fig.10, the resolution of the spectrometer is about $0.9cm^{-1}$, hence the line width above 15kOe can be ascribed to the unresolved line width.

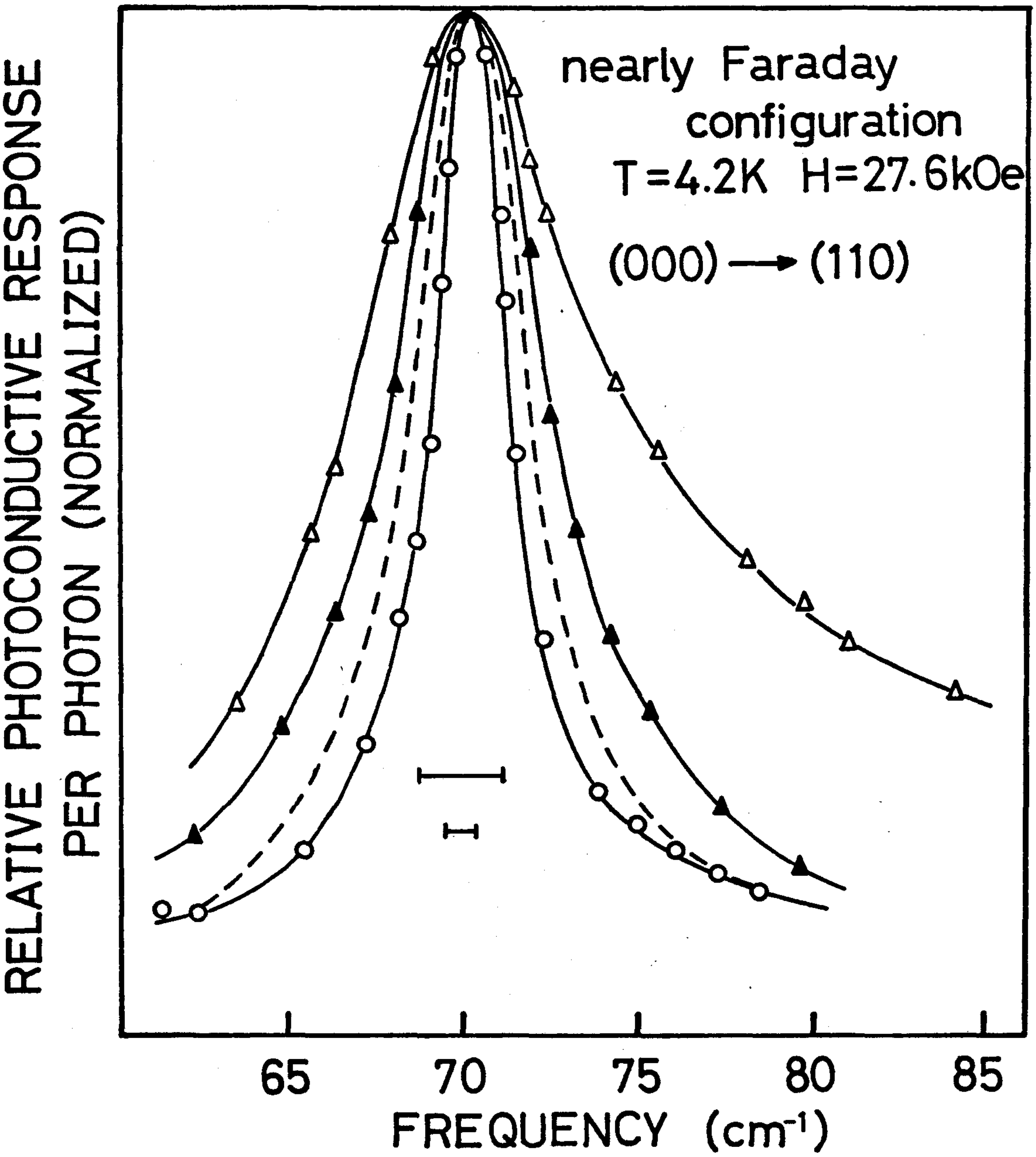

Fig.9. Normalized photoconductivity spectra correspond to the transition from (000) to (110) at 4.2K and at 27.6kOe in nearly Faraday configuration for the samples FU2015 (open triangles), FU1215 (closed triangles) and TU6114 (broken curve). The spectral resolution for the above three spectra was about 2.3cm^{-1} and the case of TU6114 with the spectral resolution of 0.9cm^{-1} is also shown by the open circles for comparison.

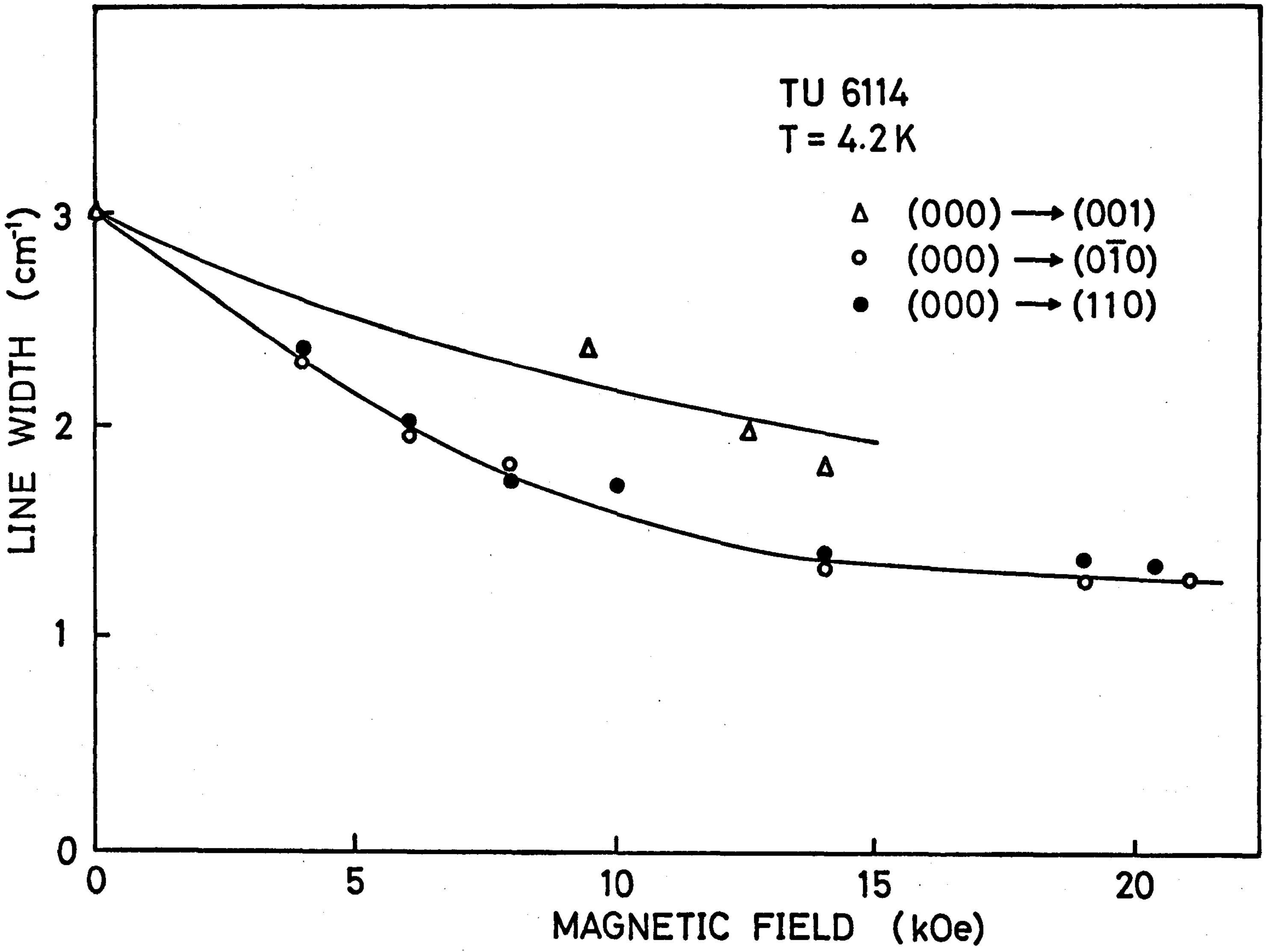

Fig.10. Magnetic field dependences of the line widths corresponding to the transitions from (000) to (001), (110) and (0$\bar{1}$0) at 4.2K (in nearly Faraday configuration). The resolving power of the spectrometer was about 0.9cm^{-1}.

The variational calculation for the donor states in magnetic field shows that the electronic wave functions of the states are shrinked with increasing magnetic field and the orbit of (001) state has a larger radius than those of (110) and $(0\bar{1}0)$ states. These magnetic field dependences of the orbit radii are calculated in the next section and shown in Figs. 12 and 13.

The mechanism of the concentration broadening of the donor spectrum is probably due to the overlapping of the electronic wave functions between the excited states of neighbouring donors. This effect cannot be neglected even in high purity specimen, TU6114, in a weak and zero magnetic field.

3-3. Theoretical considerations

(a) Calculations

The electronic states of the shallow donors in a magnetic field can be described in the effective mass approximation. The Hamiltonian operater with the magnetic field along the z-axis, using effective Rydberg ($R_y^*=m^*e^4/2\hbar^2\kappa^2$) and effective Bohr radius ($a_B^*=\kappa\hbar^2/m^*e^2$) as units of energy and length respectively can be written in the cylindrical coordinates (ρ,ϕ,z) as

$$\mathcal{H}=-\nabla^2-i\gamma\partial/\partial\phi+\gamma^2\cdot\rho^2/4-2\cdot(\rho^2+z^2)^{-1/2}, \qquad (3.3.1)$$

where magnetic field is expressed in terms of γ.

Energies of the shallow donors in the two limiting cases ($\gamma\to0$, and $\gamma\to\infty$) are solved exactly using Eq.(3.3.1). In one limiting case ($\gamma\to0$), the localized states of the electron can be described as hydrogenic states having the energies

$$E_n=-1/n^2, \qquad (n=1,2,3,\cdots\cdots). \qquad (3.3.2)$$

In another limiting case, the energies corresponding to $\gamma\to\infty$ are

$$E_{NM\lambda}=\hbar\omega_c(N+1/2)+\varepsilon_{NM\lambda}, \qquad (N=0,1,2,\cdots\cdots), \qquad (3.3.3)$$

where $\varepsilon_{NM\lambda}$ are negative discrete values for the bound impurity state.

For large and finite γ, the effective mass equation is solved approximately by means of variational calculation using trial functions of harmonic oscillator type and energies of the discrete ground and excited states are obtained. Yafet, Keyes and Adams (Y.K.A.)[27] calculated the energy of the (000) state in accordance with the scheme (NMλ) in which the ground state variational function is given by

$$F_{000} \propto \exp(-\rho^2/4a_\perp^2)\cdot\exp(-z^2/4a_{/\!/}^2), \qquad (3.3.4)$$

where $a_\perp$ and $a_{/\!/}$ are the variational parameters parallel and perpendicular to the magnetic field. Wallis and Bowlden (W.B.)$^{33)}$ extended the theory of Y.K.A. to the excited levels by replacing one variational parameter, $a_\perp$, with the cyclotron orbit, therefore their theory shows good approximation only in the range of $\gamma>10$.

In the experiment for GaAs obtained in §3-2, the highest field is 27.6kOe, which corresponds to the value of $\gamma=0.41$, therefore theoretical calculations for low and intermediate fields are required for comparison with the experimental results. To the extent of our present knowledge, the trial function proposed by Larsen$^{31)}$ should give the most reliable eigenvalues in the case of low and intermediate magnetic fields. However, the calculations will be very complicated for high energy levels, because the required integrations cannot be performed analytically. Therefore, we adopted for high field the type of trial function used by Y.K.A. for the (000) state with generalization for higher energy levels. Since for low magnetic field the Y.K.A. type functions are not appropriate for the low levels such as (000), ($0\bar{1}0$), (001), (110), we adopt for low field the trial functions used by Kohn and Luttinger (K.L.)$^{32)}$ who considered the case of zero field. The Y.K.A. type trial functions (harmonic oscillator type functions) were constructed in the present calculations referring to W.B.$^{33)}$ as follows;

$$F_{NM\lambda}(\sigma,\phi,z)=C_0\exp(iM\phi)\cdot\sigma^{|M|/2}\cdot e^{-\sigma/2}\,L^{|M|}_{N-(1/2)\cdot(M-|M|)}\cdot$$
$$\cdot P_\lambda(z)\cdot\exp(-z^2/4a_{/\!/}^2), \qquad (3.3.5)$$

where $\sigma=\rho^2/2a_{\perp}^2$, $L^{|M|}_{N-(1/2)(M-|M|)}$ is the Laguerre polynomial and $P_{\lambda}(z)$ is a polynomial given in the W.B. paper.33) In Table 2 are listed Y.K.A. type and K.L. type (hydrogenic type) trial functions used in the present variational calculation. (A similar procedure was followed by Nisida and Horii30) for Ge and they calculated the levels (000), $(0\bar{1}0)$, (001), (110), $(0\bar{1}2)$, and (112), and they reffered to the relation of Boyle and Howard.34)

The best values of the variational parameters parallel and perpendicular, $a_{/\!/}$ and $a_{\perp}$ to the magnetic field which are related to the spreadings of the electronic wave functions, are obtained and shown in Figs.11∿14 (Refer to Appendices A and B). Solid lines and broken lines in Fig.15 represent the energy values obtained in the present calculation using the Y.K.A. type and K.L. type trial functions, respectively.
To obtain the frequency values, dielectric constant $\kappa=12.6$ and effective mass $m^*=0.067m_0$ were used. The latter was derived from our experimental results for the energy difference between the transitions $(000)\rightarrow(110)$ and $(000)\rightarrow(0\bar{1}0)$.

The transition from the low field approximation to the strong field approximation occured at lower fields for higher states and the lower parts of the two calculated energy lines were joined because the true energy values should closer to the lower parts of the two lines. Furthermore for the comparison of the present results with the calculations based on the Larsen type functions, the energy of (000) in Larsen's paper31) and energies of 2p(m=±1) (or $(0\bar{1}0)$ and (110)) in the paper of Stillman et al.19) are reproduced by closed circles in the same figure, where, however, the values m^* and κ in their papers have been replaced by our values. We see that these points fall closely on our lower energy curves.

Table 2. Trial functions for the present variational calculations in cylindrical coordinates.
[$f_1(\rho, z) = \exp\{-(\rho^2/4a_\perp^2 + z^2/4a_{/\!/}^2)\}$ and $f_2(\rho, z) = \exp\{-(\rho^2/a_\perp^2 + z^2/a_{/\!/}^2)^{1/2}\}$].

(*nlm*)	(*NM*λ)	Yafet–Keyes–Adams type trial functions $F_{NM\lambda}(\rho, z, \phi)$	Kohn–Luttinger type trial functions $F'_{NM\lambda}(\rho, z, \phi)$
	210	$(1 - C\rho^2)\rho f_1(\rho, z)e^{i\phi}$	
	101	$(1 - C\rho^2)zf_1(\rho, z)$	
	$1\bar{1}0$	$(1 - C\rho^2)\rho f_1(\rho, z)e^{-i\phi}$	
	112	$(1 - Cz^2)\rho f_1(\rho, z)e^{i\phi}$	
	$0\bar{1}2$	$(1 - Cz^2)\rho f_1(\rho, z)e^{-i\phi}$	
2*p* (*m* = +1)	110	$\rho f_1(\rho, z)e^{i\phi}$	$\rho f_2(\rho, z)e^{i\phi}$
2*p* (*m* = 0)	001	$zf_1(\rho, z)$	$zf_2(\rho, z)$
2*p* (*m* = −1)	$0\bar{1}0$	$\rho f_1(\rho, z)e^{-i\phi}$	$\rho f_2(\rho, z)e^{-i\phi}$
1*s*	000	$f_1(\rho, z)$	$f_2(\rho, z)$

* The constants *C* are determined as the function being orthogonalized to the 2*p* functions at a given field.

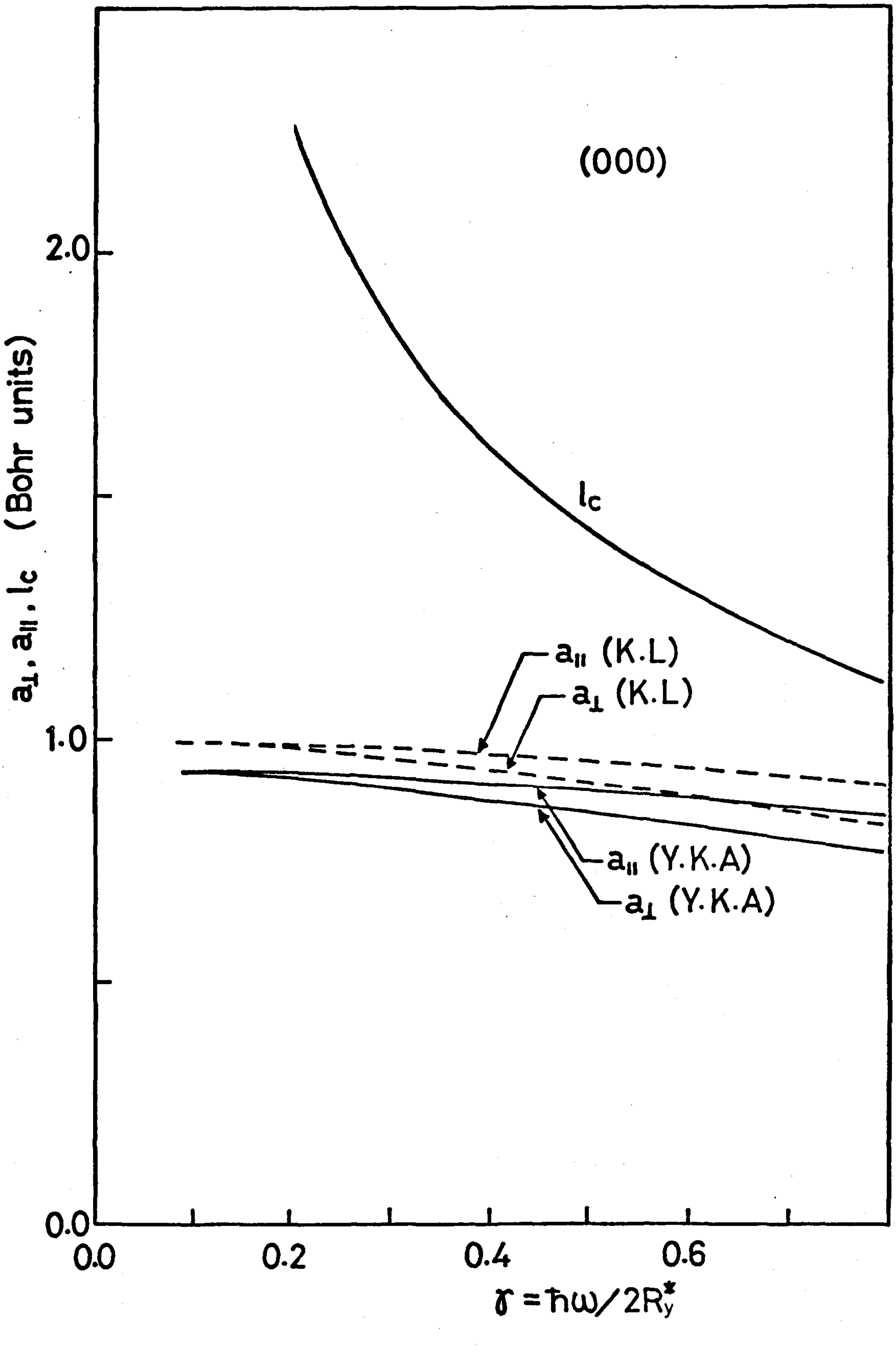

Fig.11. The best values for the parameter $a_\perp$ and $a_\parallel$ of Y.K.A. type wave function (solid curves) and K.L. type wave function (broken curves) for (000) state, together with the cyclotron radius ℓ_c as functions of the magnetic field (γ). These parameters are obtained by the variation method.

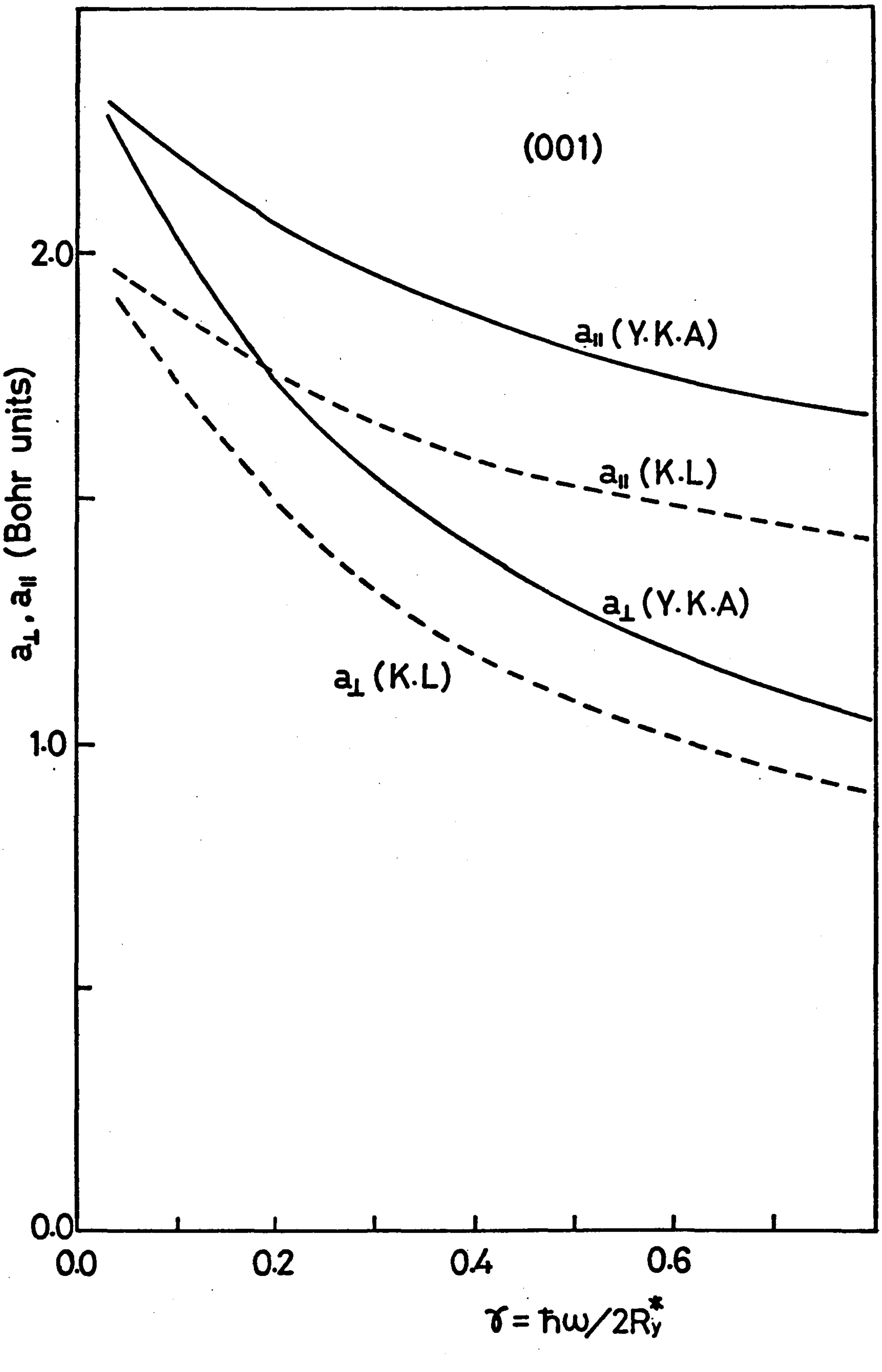

Fig.12. The best values for the parameter $a_\perp$ and $a_\parallel$ of Y.K.A. type wave function (solid curves) and K.L. type wave function (broken curves) for (001) state as functions of the magnetic field (γ).

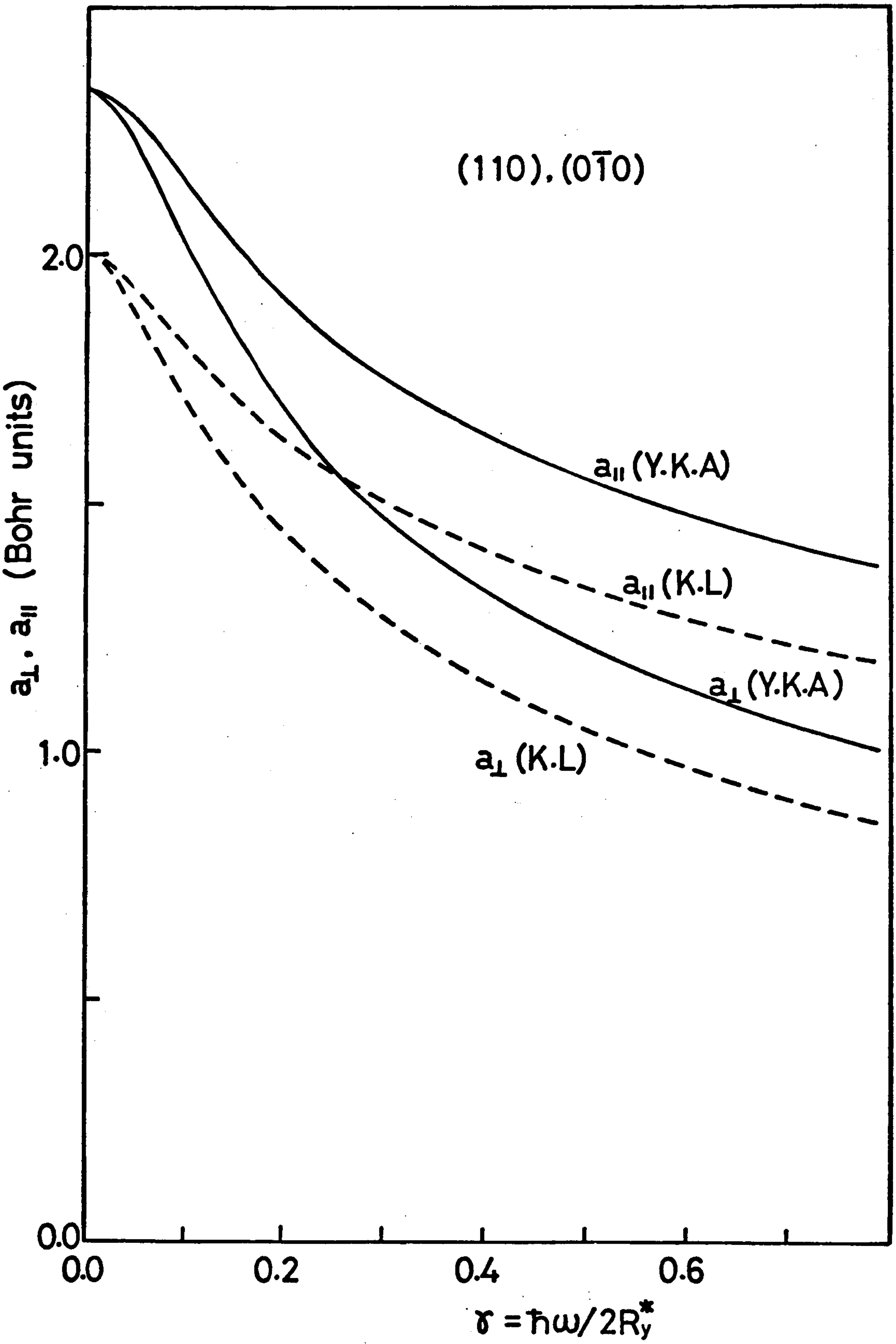

Fig.13. The best values for the parameter $a_\perp$ and $a_{/\!/}$ of Y.K.A. type wave function (solid curves) and K.L. type wave function (broken curves) for (110) and (01̄0) state as functions of the magnetic field (γ).

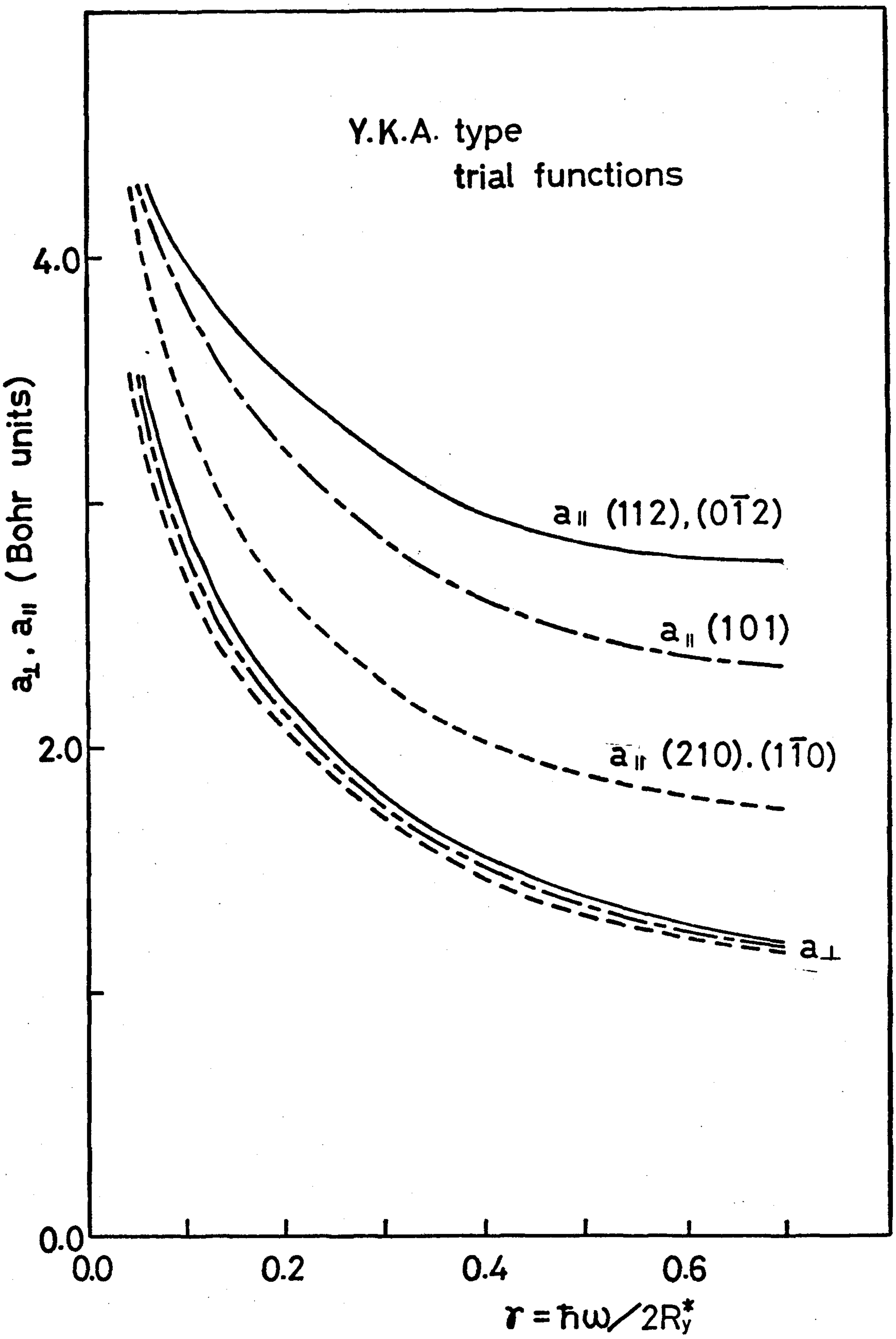

Fig.14. The best values for the parameter $a_{\perp}$ and $a_{/\!/}$ of Y.K.A. type wave function for (112), $(0\bar{1}2)$ state, (101) state and (210), $(1\bar{1}0)$ state as functions of the magnetic field (γ).

]

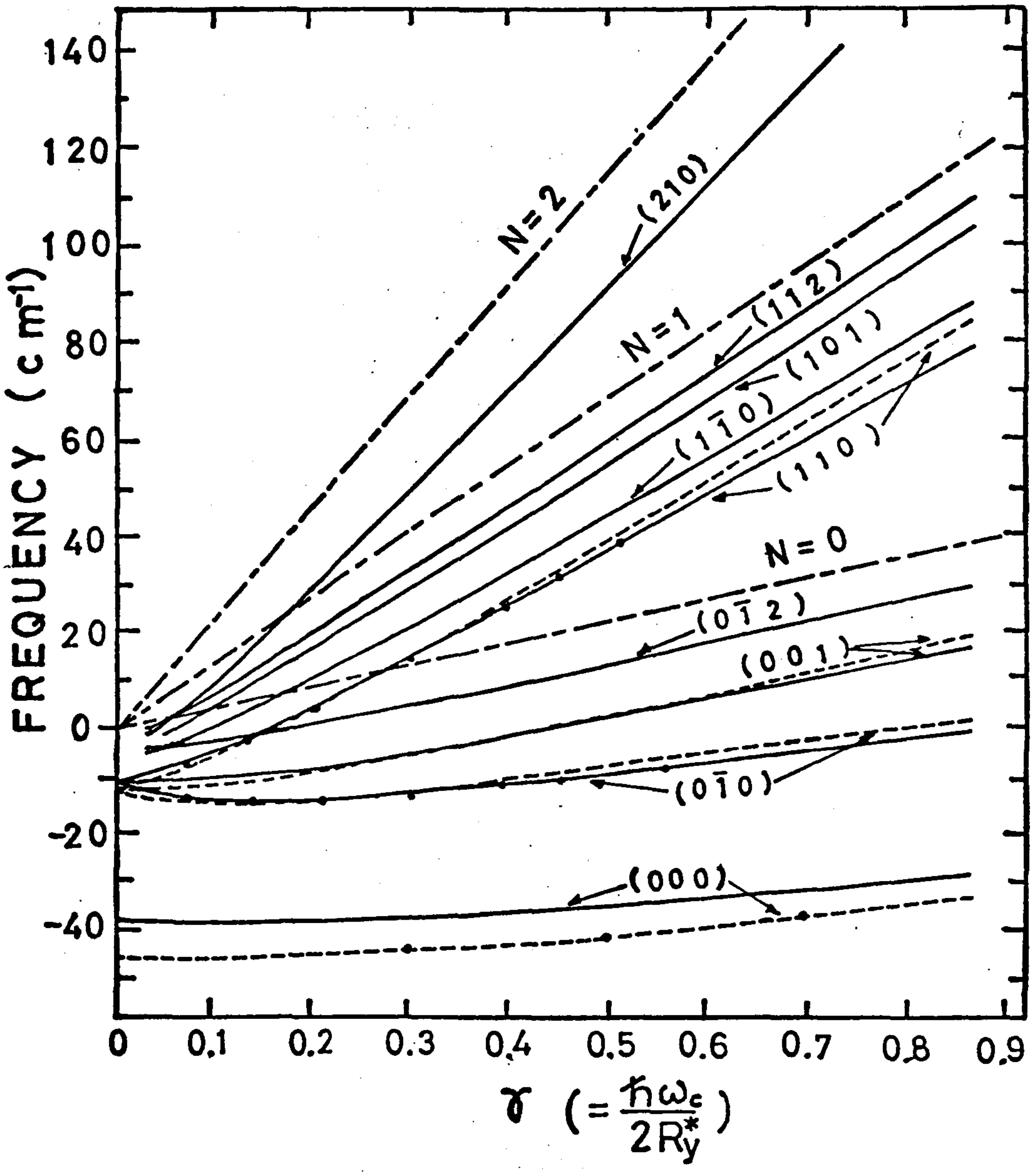

Fig.15. Computed energies for the levels (000), (0$\bar{1}$0), (001), (110), (1$\bar{1}$0), (101), (210), (112), and (0$\bar{1}$2) as functions of γ. Solid curves are from variational calculations using Y.K.A. type trial functions and broken curves from that using K.L. type functions. Closed circles are the reproduction of the values from the paper of Larsen[31)] and Stillman et al.[19)] obtained using Larsen type trial functions. The first three Landau levels are also shown.

(b) Comparison with experiment

The calculated transition energies in Fig.7 (solid curves) are compared with experimental results. The assignement of the second-lowest energy peak in the figure by Stillman et al.[19)] and Kaplan et al.[18)] as the transition 1s→2p(m=0) or (000)→(001) is supported by the present calculation. Also, the highest and the third-highest energy peaks hitherto assigned as the transitions (000)→(210) and (000)→$(1\bar{1}0)$ or 1s→3p(m=±1) are well explained by the present calculation using harmonic oscillator type (Y.K.A. type) trial functions. On the other hand, while the experimental energy values for the peak assigned as 1s→3p(m=0) by Stillman et al.[19)] are expected to fall on the calculated line for (000)→(101) if the correspondence due to Kleiner[28)] and Elliott-Loudon[29)] is correct, they fall in actuality on the calculated line for (000)→(112), and this substantiates the nonzero Δm for the peak C mentioned in association with Fig.8. The level (112) is considered corresponding to 4f(m=1) according to the relations (3.1.2). The photoconductivity peak corresponding to the calculated line for (000)→(101) could not be found in our spectra both in Faraday and Voigt configurations, and it is also absent in the spectra obtained by Stillman et al.[19)]. With regard to the intensities of the photoconductive responses for (000)→(112) and (000)→(210), we found that these are almost equally intense up to 15kOe, whereas in higher magnetic fields the latter becomes appreciably stronger than the former.

In conclusion, the use of the high field symbol (NMλ) may be preferable to the low field symbol (nℓm), even in the common magnetic field range ($\gamma>0.1$), since not only the one-to-one correspondence between (NMλ) and (nℓm) has already been established for the lower levels (000),

$(0\bar{1}0)$, (001), and (110), but also in the present study the behavior of the higher energy levels in magnetic field is well explained by the harmonic oscillator representations.

§4. Photoconductivity mechanism

Generally, photons absorbed in a semiconductor induce electronic transitions, which may arise changes of electrical conductivity. Photoconductivity measurements in a magnetic field discussed in the last chapter made clear that a part of the far-infrared photoconductivities in a epitaxial GaAs is due to the electronic transitions between the ground state and the excited states of the shallow donors.

In this chapter, the mechanisms of photoconductivities produced by higher and lower energy excitation than the ionization energy will be discussed.

4-1. Preliminaries

(a) Extrinsic photoconductivity by higher energy excitation than the ionization energy[35)]

Let us consider a semiconductor containing donors of concentration N_D and of ionization energy E_D, and acceptors of concentration N_A. Then the electron concentration in the donors is to be (N_D-N_A-n), where n is the electron concentration in the conduction band.

Suppose that a photoconductor receives radiation of energy $h\nu>E_D$, a fraction of irradiated photons are absorbed by the impurity centers in the photoconductor and the centers are ionized. The rate of recombination of electrons in the conduction band increases with increasing the electron concentration until a steady state is made, while the concentration of electrons in the conduction band is assumed to change from n to $n+\Delta n$. Then, the corresponding change in conductivity is represented by

$$\Delta\sigma=e(\mu_c-\mu_i)\Delta n, \tag{4.1.1}$$

where -e is the electronic charge, μ_c and μ_i the mobility of the electrons in the conduction band and that in the impurity states or band respectively. Thus the conductivity is given by

$$\begin{aligned}\sigma&=e\{\mu_i(N_D-N_A-n-\Delta n)+\mu_c(n+\Delta n)\}\\ &\fallingdotseq e\{\mu_i(N_D-N_A-n)+\mu_c n\}.\end{aligned} \tag{4.1.2}$$

In the last form Δn is reasonably assumed to be very small compared with n and N_D-N_A-n, and as in liquid He temperatures the impurity conduction becomes large, $\mu_i(N_D-N_A-n)$ can not be neglected comparing with $\mu_c n$. On the other hand, the resistance of the photoconductor is written as

$$R=\ell/\sigma WT, \tag{4.1.3}$$

where W and T the transverse dimensions of the sample to the longitudinal current density and ℓ the sample length.

In a limit of current obeying the Ohm's law, constant current through the sample produces a signal voltage ΔV represented by

$$\begin{aligned}\Delta V&=\frac{dV}{dR}\cdot\frac{dR}{d\sigma}\cdot\Delta\sigma\\ &=-I\cdot\frac{R}{\sigma}\cdot\Delta\sigma\\ &=-V\cdot\rho\cdot\Delta\sigma\\ &=-eV\rho(\mu_c-\mu_i)\cdot\Delta n,\end{aligned} \tag{4.1.4}$$

where we use Eqs.(4.1.1) and (4.1.3). In Eq.(4.1.4), ρ means the resistivity of the photoconductor and $\rho=\sigma^{-1}$. Δn is the fraction of the generation and recombination of the free carrier n in the rate equation, that is;

$$\begin{aligned}d(n+\Delta n)/dt=&A_T(N_D-N_A-n-\Delta n)+A_I(n+\Delta n)(N_D-N_A-n-\Delta n)+A_p(N_D-N_A-n-\Delta n)+\\ &-B_T(n+\Delta n)(N_A+n+\Delta n)-B_I(n+\Delta n)^2(N_A+n)+\\ &-B_p(n+\Delta n)(N_A+n+\Delta n).\end{aligned} \tag{4.1.5}$$

In this equation the first three termes of the right hand side represent the generation processes of the carrier, the first term $A_T(N_D-N_A-n-\Delta n)$ is the rate of excitation of electrons in the donors to the conduction band thermally and by photons of back-ground radiation, the second term $A_I(n+\Delta n)(N_D-N_A-n-\Delta n)$ represents the rate of the impact ionization of the impurity centers in the conduction band, the third term $A_p(N_D-N_A-n-\Delta n)$ gives the rate of the excitation of the electrons in the donors by far-infrared radiation. The latter three termes are concerned with the three recombination processes corresponding to the former three generation processes. That is; $B_T(n+\Delta n)(N_A+n+\Delta n)$ is the rate of capture of electrons by the empty donor centers and in the process the energy is transfered to lattice vibration.

$B_I(n+\Delta n)^2(N_A+n)$ is the rate of impact recombination and the energy is transfered to another free electron. The last term represents a radiative recombination by emitting far-infrared photons.

In the photoconductivity measurements in usual semiconductors, such as Si, Ge and GaAs, the following several conditions are satisfied.

1) Without radiation ($A_p=B_p=0$, $\Delta n=0$), n is in the steady state $dn/dt=0$.
2) In liquid He temperatures, n and Δn is very small compared with N_D-N_A and N_A, and the coefficient B_p in Eq.(4.1.5) can be neglected in comparison with the coefficient B_T.
3) In a sufficiently low applied electric field, A_I and B_I can be neglected.

Therefore, in Si, Ge and GaAs, Eq.(4.1.5) can be simplified to

$$\frac{d(\Delta n)}{dt}=A_p(N_D-N_A)-B_TN_A\Delta n, \qquad (4.1.6)$$

and in a steady state, Δn is given by

$$\Delta n = A_p(N_D - N_A)/B_T N_A, \qquad (4.1.7)$$

and B_T will be called recombination constant hereafter. Thus we obtain the signal voltage produced in the photoconductor by the radiation of energy $h\nu > E_D$ by replacing Δn in Eq.(4.1.4) with that of Eq.(4.1.7) as

$$\Delta V = -eV\rho(\mu_c - \mu_i)A_p(N_D - N_A)/B_T N_A. \qquad (4.1.8)$$

(b) Extrinsic photoconductivity by lower energy excitation than the ionization energy.

Extrinsic photoconductivity by lower energy excitation than the ionization energy is classified into three types.

1) In high purity specimens, electrons may be conductive only in the conduction band. Therefore electrons transfered from the ground state to the excited state by the photons of radiation can contribute to the photoconductivity by being promoted to the conduction band through the processes of the interactions with phonons or by applied electric field. These processes are called "photo-thermal ionization"[10) and "photo-impact ionization".[36)

Generally, the probability of the photo-impact ionization is much less than that of the photo-thermal ionization in a low applied electric field.

The electrons excited up to the excited state successibly absorb or emit phonons until they are finally captured by the ground state or elevated up to the conduction band. The latter is the general photo=thermal ionization process. The thermal ionization probability of the excited electron $I_{n\ell}$ is expressed by measurable parameters as follows;

let $R_{n\ell}$, and R_c be the photoconductive response of the specimen for the radiations having the energies from the ground state to the $n\ell$ excited state $E_{n\ell}$ and that to the bottom of the conduction band E_c, $\sigma_{n\ell}$ and σ_c the cross sections of a photon having the energies $E_{n\ell}$ and E_c respectiely to the electron in the ground state and k a constant. Then we have

$$R_{n\ell}=k\sigma_{n\ell}I_{n\ell}, \tag{4.1.9}$$

and

$$R_c=k\sigma_c. \tag{4.1.10}$$

From the above two relations, we have

$$I_{n\ell}=R_{n\ell}\sigma_c/R_c\sigma_{n\ell}. \tag{4.1.11}$$

The measurements of photoconductivity due to the photo-thermal ionization have been carried out in Ge$^{10,11,37)}$ and in high purity GaAs.$^{38)}$ But the sufficient theoretical analysis have not been carried out and the carrier concentration dependence of the photoconductivity due to photo-thermal ionization have not been reported.

2) In n-type impurity doped specimens, the activation energy of the donors, estimated from the transport properties, becomes lower than the ionization energy of the isolated donor$^{1,16)}$ with increasing donor concentration.

Some investigators have advocated the stability of the negatively charged donors D^- states$^{1)}$ and supposed that in highly doped specimens the states form so called D^- band$^{39)}$ which is considered as a conductive band. Wave functions of the excited states spread larger than that of the ground state, therefore conduction in a excited state-band$^{40,41)}$ or hopping conduction[1,16,42] through excited state may take place even for the intermediate and relatively low donor concentration range. However conduction in the excited state-band and hopping conduction necessiate a high donor concentration as well as its high compensation by acceptors, because these conduction are possible only through the ionized donor states.

Mobilities of the electrons in the D^- band, those in the excited state-band,and those for the hopping conduction are supposed to be usually very lower compairing to the mobility of the electrons in the conduction band. Therefore we can observe those three electronic conduction only in very low temperatures. However the photoconductivities due to the above three mechanisms have not been reported.

3) Recently, Nagasaka and Narita[11] proposed another photoconductive mechanism in the energy region below the ionization energy of the isolated donor in their experiment in antimony doped Ge with donor concentration more than $1\times10^{14}cm^{-3}$ at 1.6K and they named it "residual photoconductivity" (R.P.C.).

Their R.P.C. spectra show no remarkable structure over a wide energy region and also have little temperature dependence, and moreover they observed many dips in the spectrum at the energies corresponding to the photo-thermal transitions. They explained their R.P.C. spectra by using the following model; the donor impurities are distributed at random in Ge, and some donors are isolated from each other and some donors form donor-molecules and donor-clusters, such as two, three and four donor assemblies, and the ionization energies of the donor assemblies becomes lower comparing to the ionization energy of the isolated donor and distribute over a wide energy region.

4-2. Electrical measurements

The temperature dependences of the resistivity ρ, and the Hall coefficient, R_H, of several samples in dark conditions are shown in Fig.16. Apparent activation energies of the donors are obtained from the slopes of the resistivity versus reciprocal temperature curves of the samples as ε_1 (from the higher temperature region) and ε_3 (from the lower temperature region). In the ε_3 region, electronic conduction by phonon assisted hopping is dominant.42) Two kinds of carriers, electrons in the impurity states and those in the conduction band contribute to the conduction and the conduction through the impurity states becomes hardly negligible comparing to the conduction through the conduction band at liquid He temperatures.

The mobility of the electrons in the conduction band and that in the impurity states are estimated from the data shown in Fig.16, by the aid of the two-carrier-model.4) Let n_c, μ_c, n_i and μ_i be the concentrations and the mobilities of the electrons in the conduction band c and the impurity states i. Assuming that the Hall mobility is equal to the drift mobility, the Hall coefficient and the resistivity are expressed by

$$R_H/R_\infty=(1+x)(1+xb^2)/(1+xb)^2, \qquad (4.2.1)$$

$$\rho/\rho_c=(1+x)b/(1+xb), \qquad (4.2.2)$$

where $x=n_c/n_i$ and $b=\mu_c/\mu_i$ and we have the relations $n_c+n_i=N_D-N_A=n_0$, $R_\infty=1/n_0e$, and $\rho_c=1/n_0e\mu_c$. Provided b is practically constant while x is largely varied with temperature, R_H has its maximum value R_m at $xb=1$ at temperature $T=T^*$. Thus the electron mobility in the conduction band and that in the impurity states at the temperature, T^*, are expressed by

$$\mu_c = 2R_m/\rho^*; \qquad (4.2.3)$$

$$\mu_i = R_\infty/2\rho^*; \qquad (4.2.4)$$

where ρ^* is the resistivity at $T = T^*$.
and the numerical results are listed in Table 1.

The current density J vs electric field E curves of the various specimens are obtained at liquid He temperatures under a constant back ground radiation and by the use of a constant current circuit and the data are plotted in Fig.17. Though at low current density and low electric field, the J-E curves show an ohmic behavior, in high current density region the electric field shows a saturation. Then it decreases indicating the impact ionization of the neutral shallow donor levels. The critical field of the saturation depends on the electron mobility and the compensation ratio of the donors.

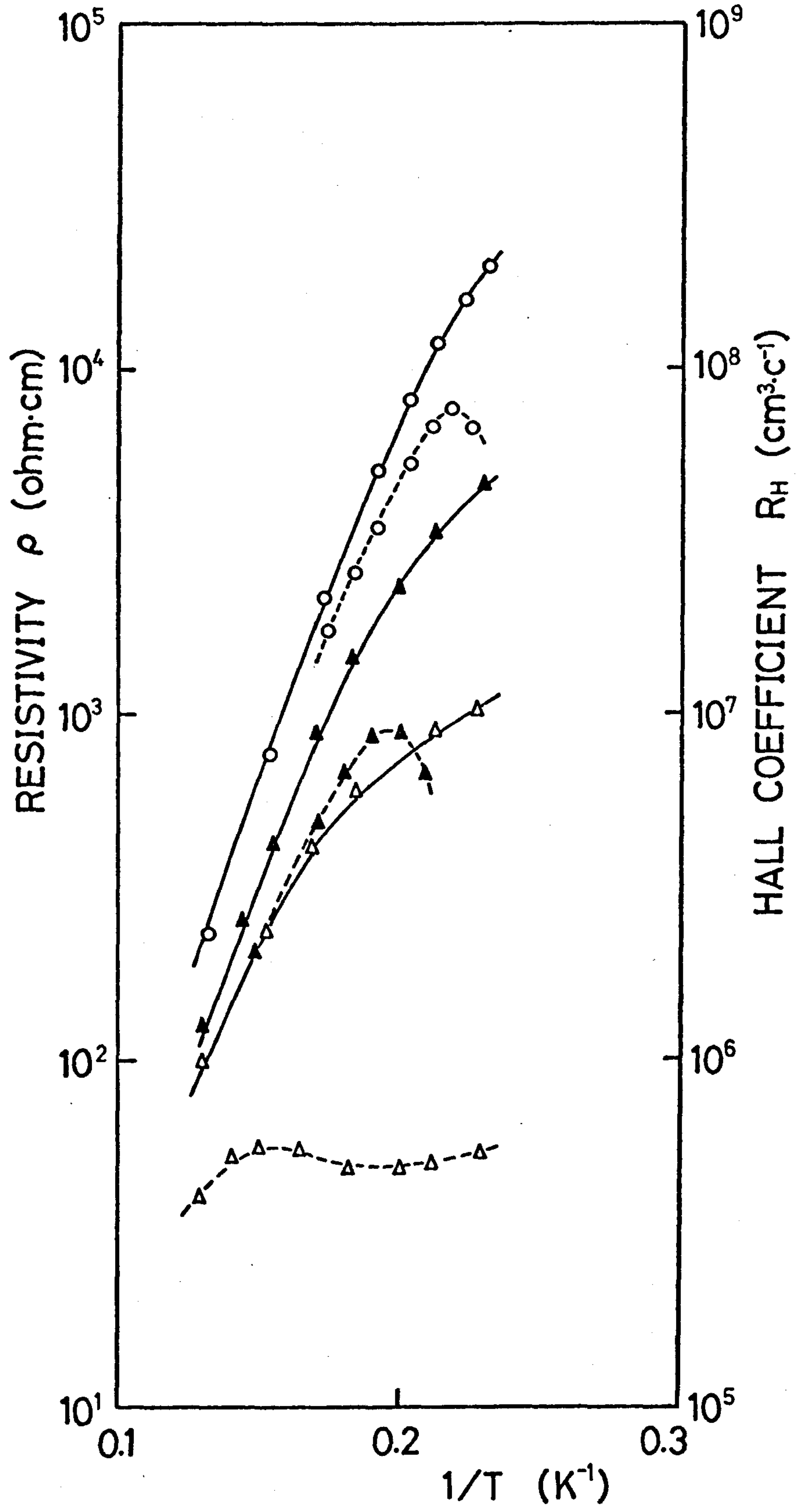

Fig.16. Temperature dependences of the Hall coefficients (broken curves) and resistivities (solid curves) for the samples TU6114 (open circles), FU1215 (closed triangles) and FU2015 (open triangles).

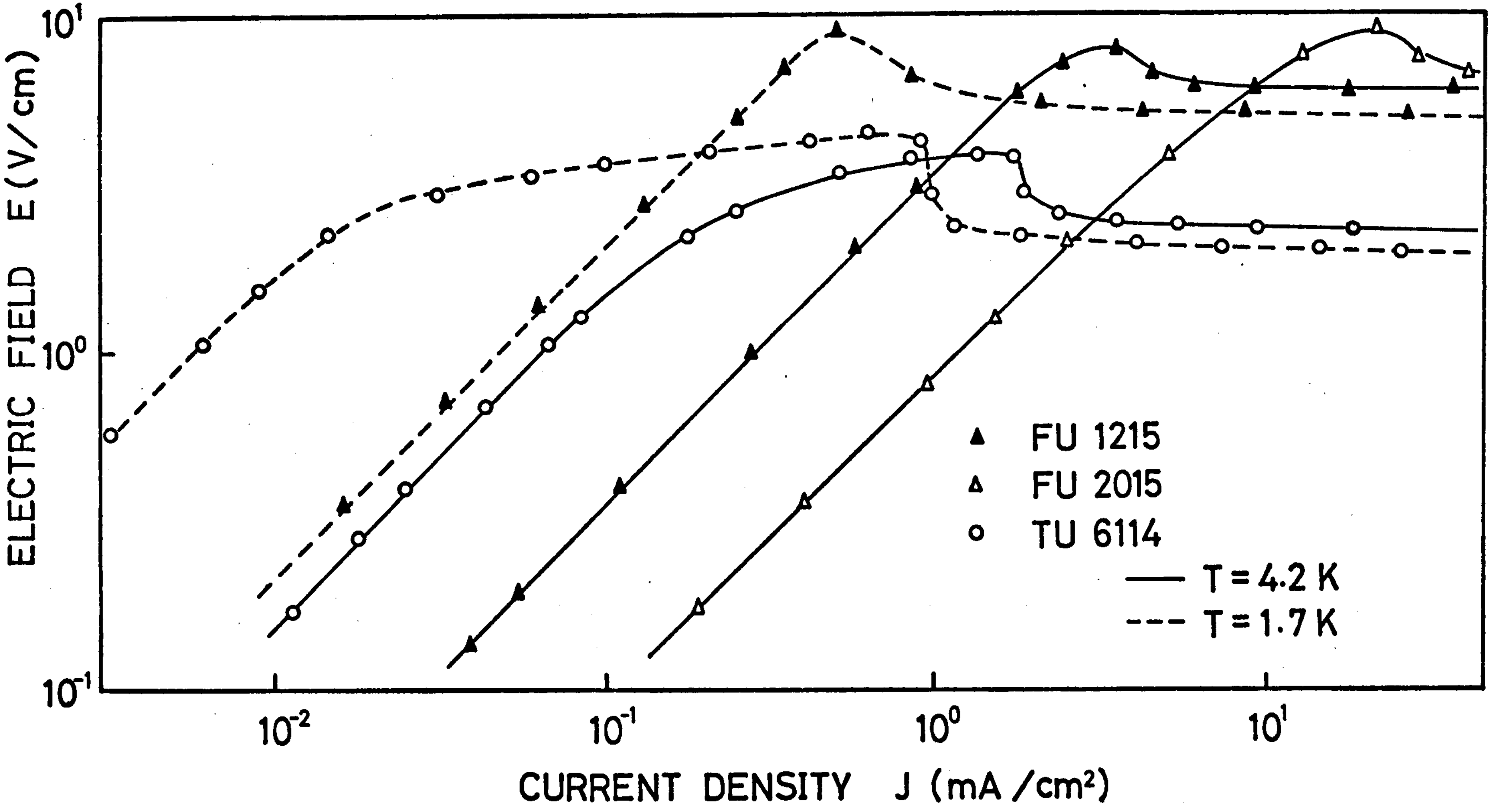

Fig.17. Current density vs electric field curves at 4.2K (solid curves) and 1.7K (broken curves) for the samples TU6114 (open circles), FU1215 (closed triangles) and FU2015 (closed triangles).

4-3. Carrier concentration and temperature dependences of photoconductivity.

In order to investigate the far-infrared extrinsic photoconductivity mechanism in epitaxial GaAs, temperature dependences and impurity concentration dependences of the photoconductive responses have been measured for the low impurity concentration samples (TU4714, TU6114) and the high impurity concentration ones (FU1215, FU2015, TU3015).

Figs.18 and 19 show the temperature dependence of photoconductivity spectra for TU4714 and FU1215 where all spectral values are normalized at about 60cm^{-1} which is larger than the ionization energy 46.3cm^{-1}. In the low impurity concentration case (TU4714), the photoconductivity spectrum is characterized by a sharp peak at 35.5cm^{-1} due to transition from the ground state (1s) to the first excited state (2p) of the shallow donor and by another small peak at about 42cm^{-1}. The photoconductivity spectrum is independent of temperature above 3.5K, however, the main photoconductivity decreases with decreasing temperature below 3K.

In the high impurity concentration case (FU1215), the position of the highest peak at 35.5cm^{-1} does not change, though the width becomes broader comparing to the case of TU4714, while the small peak at higher energy of 42cm^{-1} observed in TU4714 cannot be resolved merging into the background and the absolute value of the photoconductive response is reduced extremely. We could not observe photoconductive response for the specimen with the highest impurity concentration (TU3015). The mobilities of the electrons in the conduction band obtained from the measurements shown in Fig.16 indicate that the lowering of the mobility with increasing impurity concentration is very little. Therefore the abrupt decrease of the photoconductive response with increasing impurity

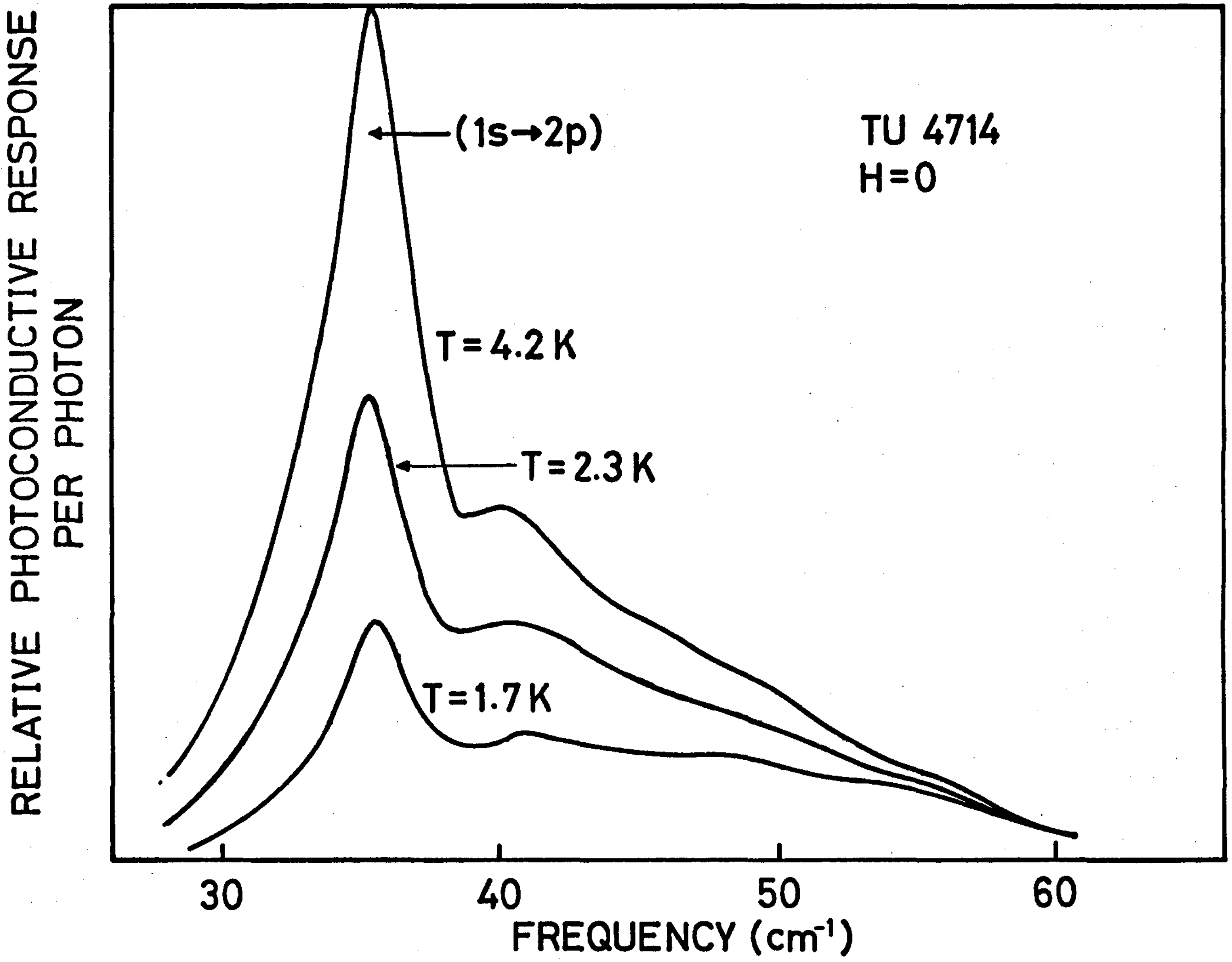

Fig.18. Photoconductivity spectra at various temperatures without magnetic field for the appreciably pure sample of TU4714. All spectral values are normalized at ∿60cm^{-1}. The impurity concentration of TU4714 is 4.7×10^{14}cm^{-3}.

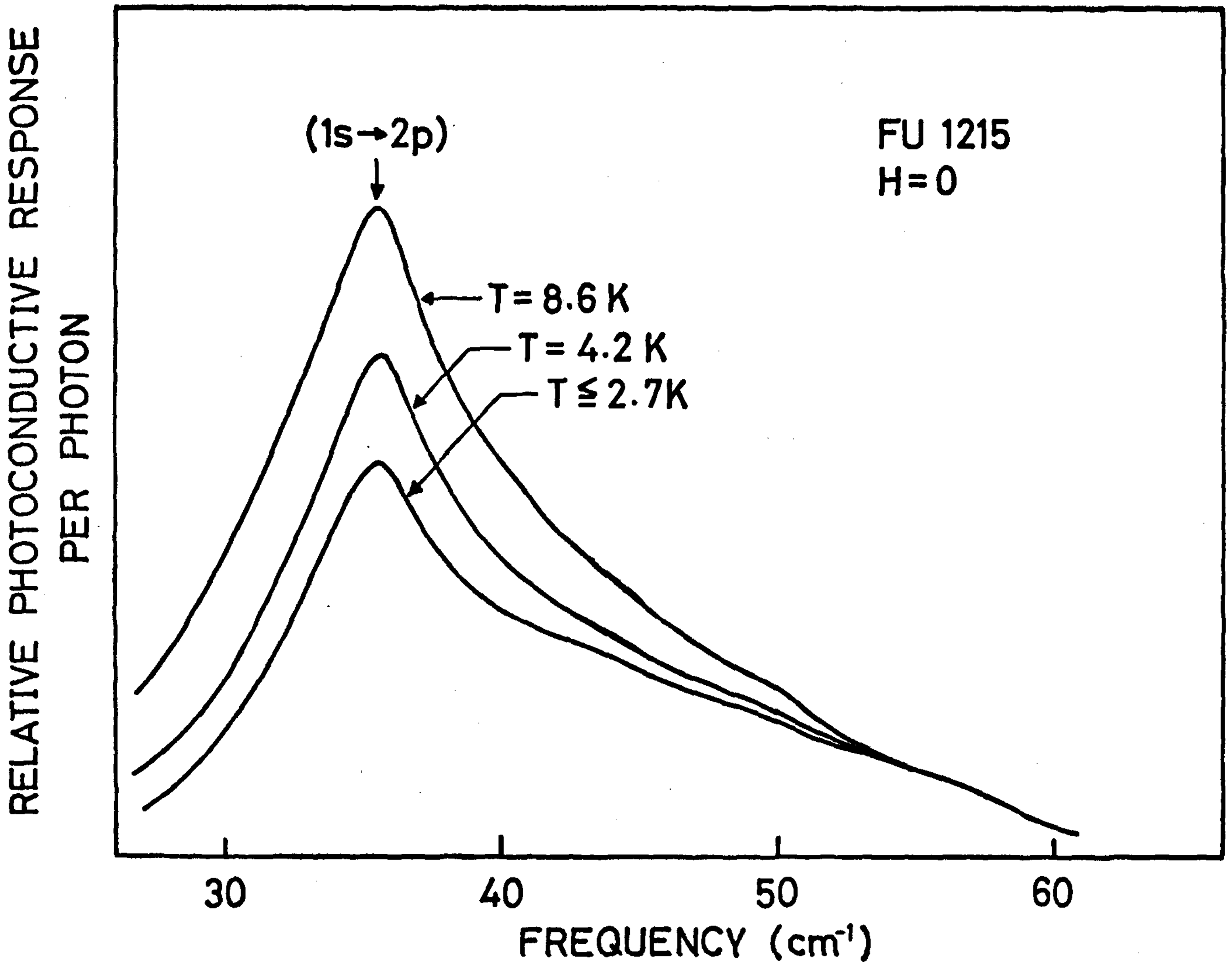

Fig.19. Photoconductivity spectra at various temperatures without magnetic field for the impure sample of FU1215. All spectral values are normalized at ∿60cm^{-1}. The impurity concentration of FU1215 is 1.2×10^{15}cm^{-3}.

concentration can not be explained by the change of the electron mobility in the conduction band. Between 8K and 4K, the photoconductivity at the main peak decreases with decreasing temperature, though the photoconductivity becomes unchanged with temperature below 2.7K.

Several physical properties derived by means of electrical and photoconductivity measurements are summarized in Fig.20, where the electron mobilities in the conduction band and the impurity state at T=T*, the line widths of the spectra associated with the transitions from the ground state to the 2p excited state in zero magnetic field and the photoconductive responses at $60\mathrm{cm}^{-1}$ are shown. For the photoconductive response we normalized the measuring value taking the resistivity of the specimen ρ, applied electric field V and thickness of specimen d into consideration.

Electric field applied to the specimen is varied in a wide temperature range in the photoconductivity measurements, for instance from 0.3V/cm ($1.7\times10^{-3}\mathrm{mA/cm^2}$) to 4.6V/cm ($0.8\mathrm{mA/cm^2}$) for TU6114, and 0.3V/cm ($1.4\times10^{-2}\mathrm{mA/cm^2}$) to 6.0V/cm ($0.36\mathrm{mA/cm^2}$) for FU1215 at 1.7K (refer to Fig.17). We found as the results that the relative photoconductivity spectrum figures are independent of applied electric field and current density.

The above results indicate that the photoconductivity associated with the excitation to the excited states are mainly due to photo-thermal ionizations except for the case of the high impurity specimen (FU1215) below 2.7K. The thermal ionization probability of electrons in the excited state can be determined by using Eq.(4.1.11). Since the photoconductivity spectrum figures are independent of temperature above 3.5K for TU4714, TU6114 and above 8K for FU1215, we conclude without the

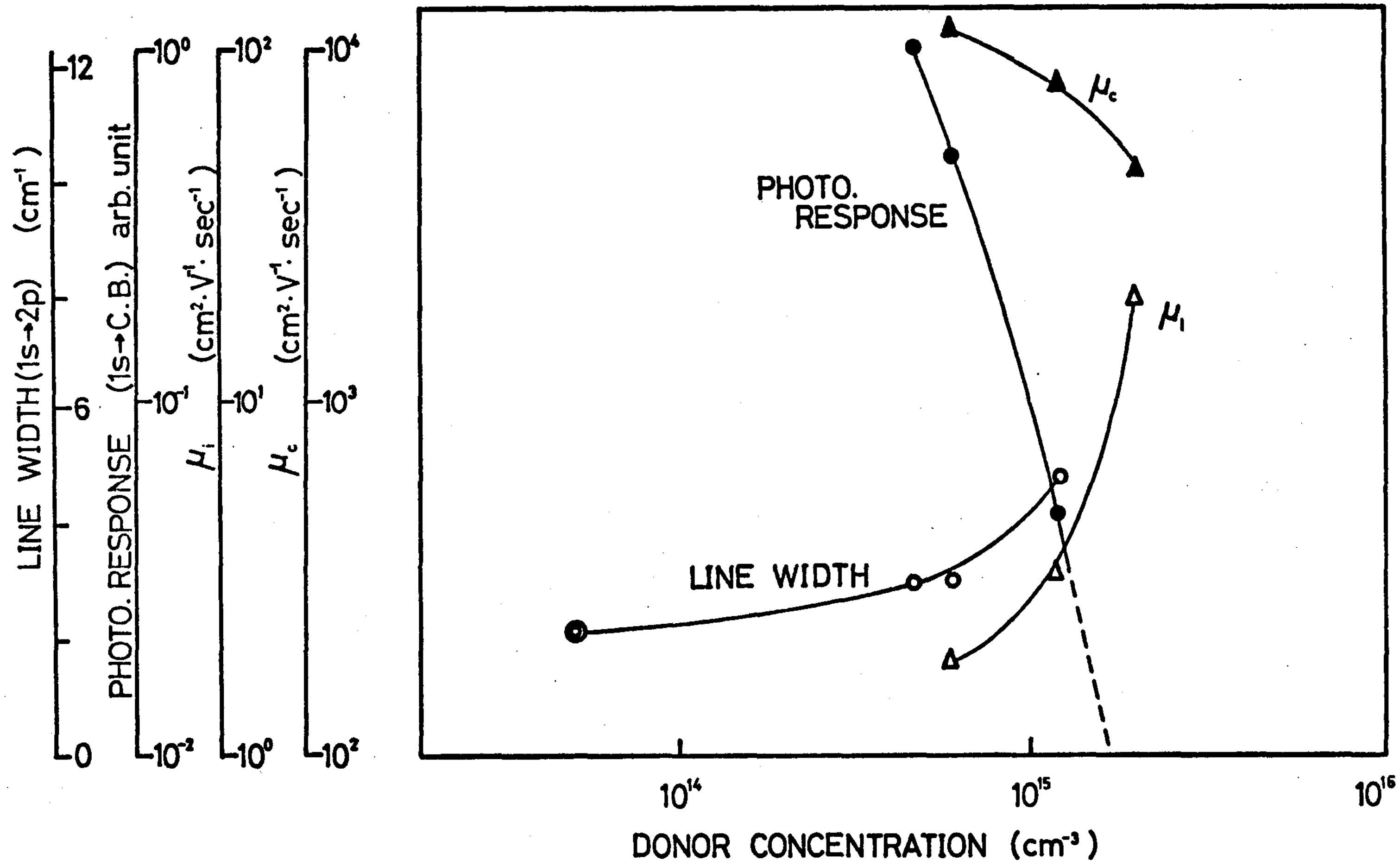

Fig.20. Donor concentration dependences of several physical properties for GaAs, electron mobility in the conduction band μ_c and impurity state μ_i at T=T* (T* are the temperatures at which the Hall coefficients have their maximum values), the line widths of the spectra associated with the transitions from the ground state to the 2p excited state at H=0kOe and the photoconductive responses at 60cm^{-1}. We normalized photoconductive responses, taking the sample resistivity ρ, applied electric field V and thickness d into consideration. Double circle is obtained from the data by Stillman et al.$^{24)}$

knowledge of the absorption cross-sections σ_c and $\sigma_{n\ell}$ that the thermal ionization probability becomes unity above the temperatures for each specimen. The phenomenon of the saturation of the photoconductivity due to the photo-thermal ionization was first observed for GaAs.38) The saturated and temperature independent photoconductivity associated with the excitation to the excited state in the high temperature region may be resulted from the fact that all of the electrons in the excited states optically excited from the ground impurity state are thermally elevated into the conduction band prior to their fall back to the ground state.

Temperature dependence of the apparent thermal ionization probability of the electrons in the 2p excited state is obtained experimentally and the data are plotted in Fig.21 ("the apparent" means that for the highly doped sample the photoconductive electron also contain those in the conductive excited band, the mobility of which may be appreciably smaller than those in the conduction band.). In the same figure, the experimental result obtained for a very high purity specimen of $N_D=4.8\times10^{13}\text{cm}^{-3}$ by Stillman et al.38) is also shown. Several remarkable features of the curves are seen in the figure.

1) The ionization (activation) energy of the 2p excited state has been believed to be able to be determined from the slope of the thermal ionization probability vs resiprocal temperature curves. Nagasaka and Narita11) carried out this method for Sb-doped Ge and considered the obtained energy as the energy separation between the bottom of the conduction band and the 2p excited state in Sb-Ge.

However in the case of GaAs, the obtained energies by the above method which are about $3.8\sim1.7\text{cm}^{-1}$ are inconsistent with that determined from the effective mass theory as the energy separation between the bottom of

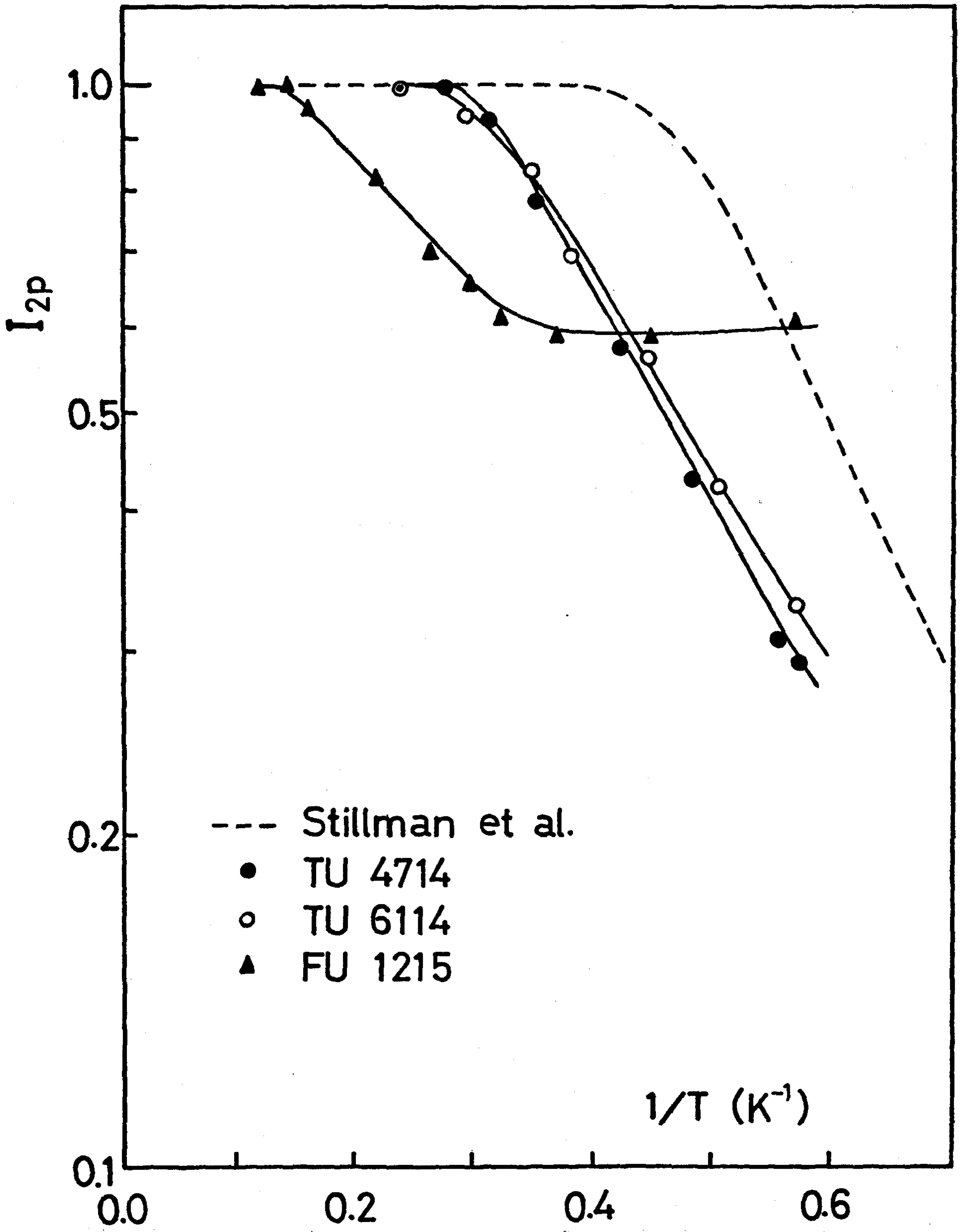

Fig.21. Temperature dependences of the apparent photo-thermal ionization probability, obtained from the ratios of the photoconductivities due to the excitation by the energy between the ground state and the 2p excited state, to those corresponding photoconductivity due to the excitation of the ionization energy for the samples TU4714 (closed circles), TU6114 (open circles), and FU1215 (closed triangles). These ratios are normalized to unity above 3.5K for TU4714, TU6114 and above 8K for FU1215, because the photoconductivities saturate above the temperature. Experimental result obtained by Stillman et al.[38] (broken curve) are also shown.

the conduction band and the 2p excited state which is about 11.6cm^{-1}. Stillman et al.[38)] supposed that the small activation energy may be attributed to large thermal ionization probability of the p-like excited state compared with that of the s-like excited state at the same energy.

2) The temperature, T_s, at which the thermal ionization probability shows saturation shifts toward high temperature side with increasing donor concentrations.

3) In high impurity concentration case (FU1215) in the low temperature region ($\leq$2.7K), the temperature dependence of the apparent photo-thermal ionization probability (the apparent activation energy) vanishes. Besides in the photoconductivity spectra, the large peak at 35.5cm^{-1} is observed even at 1.7K which corresponds to the electronic transitions from the ground state to the 2p excited state. Nagasaka and Narita[11)] have observed a photoconductivity with considerably small temperature dependence. They attributed it to the formation of the donor-molecules and this assumption was justified by its structureless and wide-wavelength spectral figure. The clear appearance of the main peak in the GaAs spectra of high impurity concentration indicate that the origin of the vanishing of the apparent activation energy of the 2p state differ from the case in Sb-Ge. The above results suggest us that the electrons in the 2p excited state becomes conductive, that is: the formation of the excited state band[40,41)] in the specimen with increasing impurity concentration. In the case of GaAs, different from that of Ge, the compensation ratio of the donors by the acceptors is appreciably large, ≈0.50 for FU1215, therefore electronic conduction through the excited state band is more probable to occure than the conduction in D^- band.[39)]

Temperature dependences of photoconductive responses for several specimens by higher energy excitation than the ionization energy are also measured under the condition of low applied electric field and they are shown in Fig.22. Excitation energy is $\sim 60\mathrm{cm}^{-1}$ and we normalized the photoconductive responses taking into account the differences of the resistivity ρ, and the thickness of specimen d, and the variation of the applied electric field V. In all the measurements, the condition of $\alpha d \ll 1$ is satisfied, where α is the absorption coefficient of the specimen.

In the low impurity concentration case (TU4714, TU6114), the normalized photoconductive responses decrease with decreasing temperature, while in the high impurity concentration case (FU1215) the normalized photoconductive responses have small temperature dependences, and especially almost zero below 3K. Temperature changes of the normalized photoconductive responses by the high energy excitation can be attributed mainly to that of the recombination constant B_T in Eq.(4.1.8), if we can neglect the impurity conduction through the excited state band, and the temperature change of the electron mobility in the conduction band.

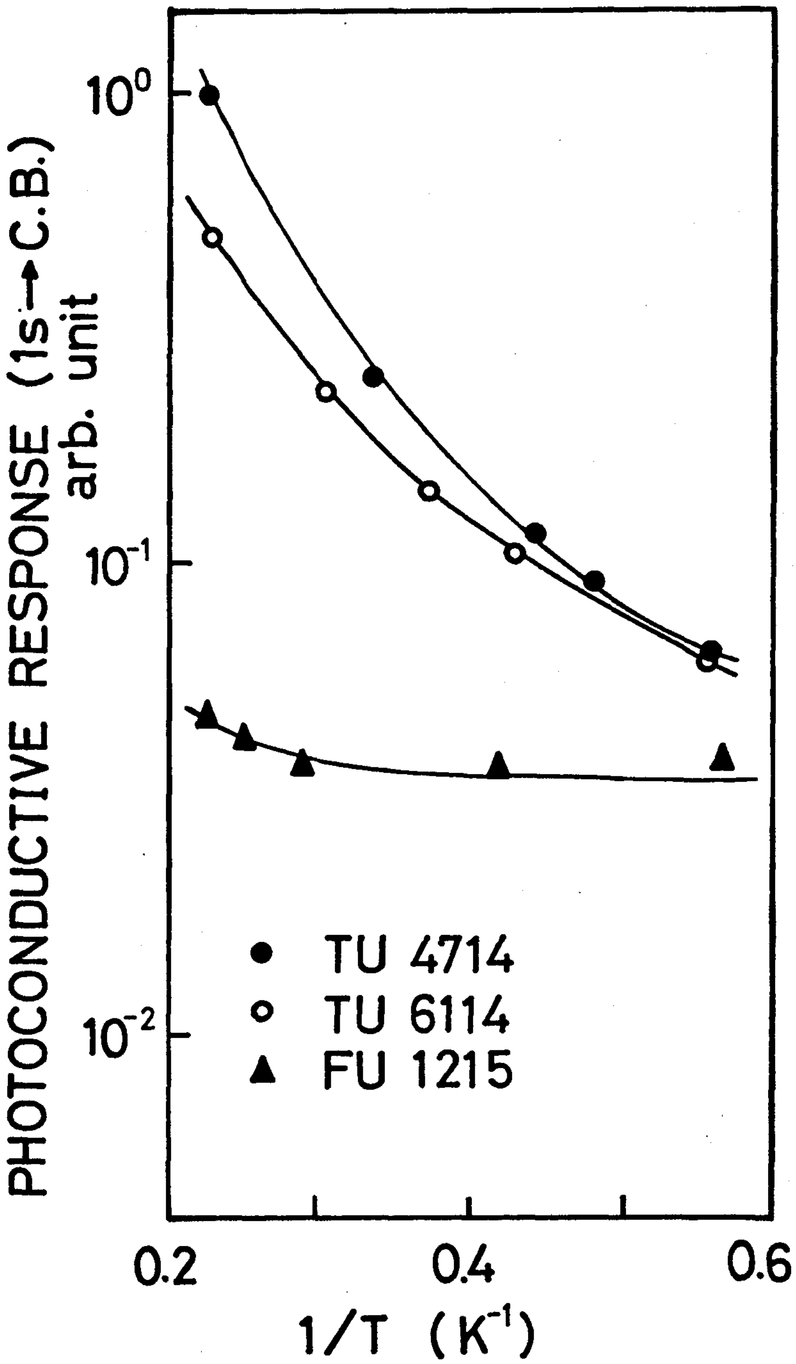

Fig.22. Experimental photoconductive responses due to the excitation of the energy 60cm^{-1} for the samples, TU4714 (closed circles), TU6114 (open circles) and FU1215 (closed triangles). We normalized these photoconductivity by taking the sample resistivity ρ, applied electric field V and thickness d into consideration.

4-4. Theoretical considerations

(a) Cascade capture model (Ascarelli-Rodriguez's model)43)

It is well known that the electronic states of shallow donors can be described much better by effective mass theory than those of other type centers. From the above reason the kinetics of the low temperature recombination of electrons in the conduction band of n-type Ge with shallow donors have attracted the interests of theorists and experimentalists of semiconductors. The recombination cross-section in Ge with As and Sb impurities, at 4K has been estimated experimentally44) to be an order of magnitude of 10^{-11} to 10^{-12} cm^2 and it varies with temperature in an approximation according to the $T^{-2.5}$ law. There are a number of recombination mechanisms of the conduction electron, one of them is a direct recombination to the ground state accompanied by light emission or phonon emission and another one is a recombination, the energy of which is transfered to another free electron (impact recombination). However, the theoretical recombination cross-sections in the above recombination process for Ge at 4K are estimated to be about $10^{-15} \sim 10^{-18} cm^2$ and also the theoretically expected temperature behavior is in considerable disagreement with experimental one.

The explanation of the above large discrepancy between the theory and the experiment is first tried classicaly by Lax45) and then the quantum-mechanical formulation was done by Ascarelli and Rodriguez (A.R.).43) The model used for the formulation is a so-called "cascade capture model". In this model, recombination occurs with the initial capture of a conduction electron in an excited donor state followed by successive transitions to lower lying states, in each transition of which a single acoustic phonon is emitted.

Thermal ionization probabilities and recombination cross-section were treated by A.R.43) as followings: Let S_j be the probability of an electron in the bound state characterized by j being never ionized into the conduction band (this probability is called "sticking probability"), $P_j^{(\nu)}$ the probability of the electron in the state j being elevated to the conduction band after ν transitions through other states, $P_{j'j}$ the probability of the electron for the transition from the bound state j to j', $w_{j'j}$ the probability of the electron in the state j being transfered to state j' $(j'\neq j)$per unit time, and β_j the probability of the state j being thermally ionized per unit time. Then we have,

$$S_j+I_j=1, \tag{4.4.1}$$

$$I_j=\sum_{\nu=1}^{\infty}P_j^{(\nu)}, \tag{4.4.2}$$

$$P_j^{(\nu)}=\sum_{j'\neq j}P_{j'j}P_{j'}^{(\nu-1)}, \tag{4.4.3}$$

$$P_{j'j}=w_{j'j}[\sum_{j'\neq j}w_{j'j}+\beta_j]^{-1}, \tag{4.4.4}$$

$$P_j^{(1)}=\beta_j[\sum_{j'\neq j}w_{j'j}+\beta_j]^{-1}. \tag{4.4.5}$$

The capture cross-sections, $\sigma_c(j)$, are related to the transition probabilities of the electron to the conduction band in the principle of detailed balancing and given by

$$\sigma_c(j)=g_i\pi^2\hbar^3\beta_j/2m^*(kT)^2\cdot\exp\{(E_c-E_j)/kT\}, \tag{4.4.6}$$

where g_i is the degeneracy of the state j, $\hbar$ Plank's constant, m* the effective mass, k Boltzman constant, T the absolute temperature and E_c and E_j are the energy of an electron at the bottom of the conduction band and in the bound state j respectively.

The cross-sections of the electron in the conduction band for the recombination, σ, is given by

$$\sigma=\sum_j \sigma_c(j)\cdot S_j, \qquad (4.4.7)$$

and recombination constant B_T in Eq.(4.1.8) is defined by

$$B_T=\sigma\cdot v_T, \qquad (4.4.8)$$

where v_T is the thermal velocity.

We can obtain the thermal ionization probability and recombination constant only by calculating $w_{j'j}$, and β_j. The calculation was given for the band of spherical effective mass with donor impurity whose bound states can be described by a hydrogenic model. The fastest transition processes are assosiated with the absorption or emission of a phonon and the electron-phonon interaction involved in the transition is treated as the deformation potential.

The Hamiltonian is given by

$$\mathcal{H}'=E_1 \mathrm{div}\vec{S}(\vec{r}), \qquad (4.4.9)$$

$$\vec{S}(\vec{r})=(\hbar/\rho V)^{1/2}\sum_{q,\mu}\vec{e}_{q,\mu}(\omega_{q,\mu})^{-1/2}a^{+}_{q,\mu}\exp(i\vec{q}\cdot\vec{r})+ \\ +\text{Hermitian conjugate}, \qquad (4.4.10)$$

where E_1 is the deformation potential and $\vec{S}(\vec{r})$ the displacement of an atom in the lattice from the equilibrium position given by $\vec{r}$, ρ and V the density and the volume of the specimen respectively, and $\vec{e}_{q,\mu}$, $\omega_{q,\mu}$, and $a^{+}_{q,\mu}$ the unit polarization vector, the angular frequency and the creation operator associated with the phonon wave vector $\vec{q}$ and the three dimensional polarization direction $\mu(\mu=1,2,3)$.

The wave function of an electron in the conduction band should be expressed as the Coulomb wave function corresponding to the wave vector $\vec{k}$ and given by

$$\phi_{\vec{k}}=V^{-1/2}(2\pi\gamma)^{1/2}[1-\exp(2\pi\gamma)]^{-1/2}\exp(i\vec{k}\cdot\vec{r})F[i\gamma,\ 1,\ i(kr-\vec{k}\cdot\vec{r})], \tag{4.4.11}$$

where $\gamma=1/\kappa a^*$, κ is the dielectric constant, a^* is the effective Bohr radius and $F(a,b,z)$ is the "confluent hypergeometric function". For the wave functions of the bound state j, only the s state functions (states with zero angular momentum) are used for simplification then the bound states are characterized only by n hereafter.

The wave functions for the bound states n are given by

$$\phi_n(\vec{r})=(\pi n^3 a^{*3})^{-1/2}\exp(-r/na^*)F(-n+1,2,2r/na^*). \tag{4.4.12}$$

Using Eq.(4.4.9)~(4.4.12), we have the expressions of $w_{n'n}$ and β_n for $n'<n$,

$$w_{n'n}=64E_1^2\hbar^4c_s^3/\pi\rho a^{*8}E_i^5\cdot(n'n)^5/(n-n')^5(n+n')^3\times$$

$$\times[1-\exp(-\hbar w_{nn'}/kT)]^{-1}, \tag{4.4.13}$$

and for $n'>n$,

$$w_{n'n}=w_{nn'}\exp(-\hbar w_{n'n}/kT), \tag{4.4.14}$$

with

$$\hbar w_{nn'}=E_i(1/n'^2-1/n^2), \tag{4.4.15}$$

and

$$\beta_n=256E_1^2m^*\hbar^2c_s^3/\pi\rho a^{*6}n^3(kT)^4\cdot\int_0^{n^2/s}dt\cdot t^3\exp(-t^{-1}-g^2t^2/n), \tag{4.4.16}$$

where $s=E_i/kT$, and $g=2\hbar c_s/a^*kT$, E_i is the ionization energy of a donor at the ground state, and c_s the sound velocity of the material.

Ascarelli and Rodriguez[43)] compared the experimental results of Ge with the calculation of the cross-section for recombination by the above mentioned method. However the agreement between the experiment and the calculation was not sufficiently good, because the energy surface of the conduction band in Ge is not spherical and moreover only single transition between excited states are taken into account. After their study, Brown and Rodriguez[47)] treated multiple transition process up to four times. Beleznay and Pataki (B.P.)[46)] extended their theory to the bound states with non-zero anguler momentum.

(b) Application of the cascade capture model to our experimental results

Experimental results described in §4-3 are summarized in the followings.

1) The activation energy determined from the photoconductivity due to the photo-thermal ionization associated with the 2p excited state is much smaller than energy separation between the bottom of the conduction band and the 2p excited state determined from the effective mass theory.

2) Photoconductive response at the $60\mathrm{cm}^{-1}$ range decreases with decreasing temperature.

3) In the high impurity concentration case (FU1215), the photoconductive response by the excitation corresponding to the energy between the ground state and 2p excited state is invariant with temperature (≤ 2.7K). This fact suggests that in the temperature range electron conduction through the 2p excited states occures.

4) With increasing donor concentration, the saturation temperature of the photoconcuctivity due to photo-thermal ionization increases.

5) Above the donor concentration of $10^{15}\mathrm{cm}^{-3}$, the photoconductive response and its temperature change become extremely small.

In this section, we first calculate the thermal ionization probability

I_n, and the recombination constant B_T in GaAs after the formulation by A.R.[43)] to explain the extrinsic photoconductivity mechanism for the specimen with low impurity concentration (the summarized experimental results (1) and (2)) and later we will proposed qualitative model to explain the experimental results for the specimen with high impurity concentration (the summarized experimental results (4) and (5)).

By Eqs.(4.4.1)∿(4.4.8) and Eqs.(4.4.13)∿(4.4.16), the sticking probability for bound states n, the thermal ionization probability for the 2s excited state and recombination constant are calculated. In this calculation the donor wave functions corresponding to s states for the donor levels n=1∿7 are used. Different from the calculation by A.R., we take into account the multiple transition of electrons between the excited states up to thirty thousands times. In the calculation the following physical values of GaAs are used; the dielectric constant $\kappa=12.6$, the effective mass $m^*=0.067m_0$, the deformation potential $E_1=8.9\text{eV}$, the sound velocity $c_s=1.88\times10^5\text{cm/sec}$ and the density of mass $\rho=5.31\text{gr/cm}^3$ (Refer to Appendices C and D).

Fig.23 shows the thermal ionization probabilities determined experimentally for the 2p excited state (the experimental result for TU4714 replotted from Fig.21) and those calculated theoretically for the 2s excited state of the same energy to the 2p state by use of the cascade capture model. In the same figure two theoretical curves calculated based on the assumption of the single electron-phonon interaction are also shown, and in these two calculations impurity states are assumed to be $n\leq7$ and $n\leq2$ respectively. Activation energies determined from these two theoretical curves below 3K are nearly equal to the energy separation between the 2s excited state and the bottom of the conduction band and are much larger than the experimental one.

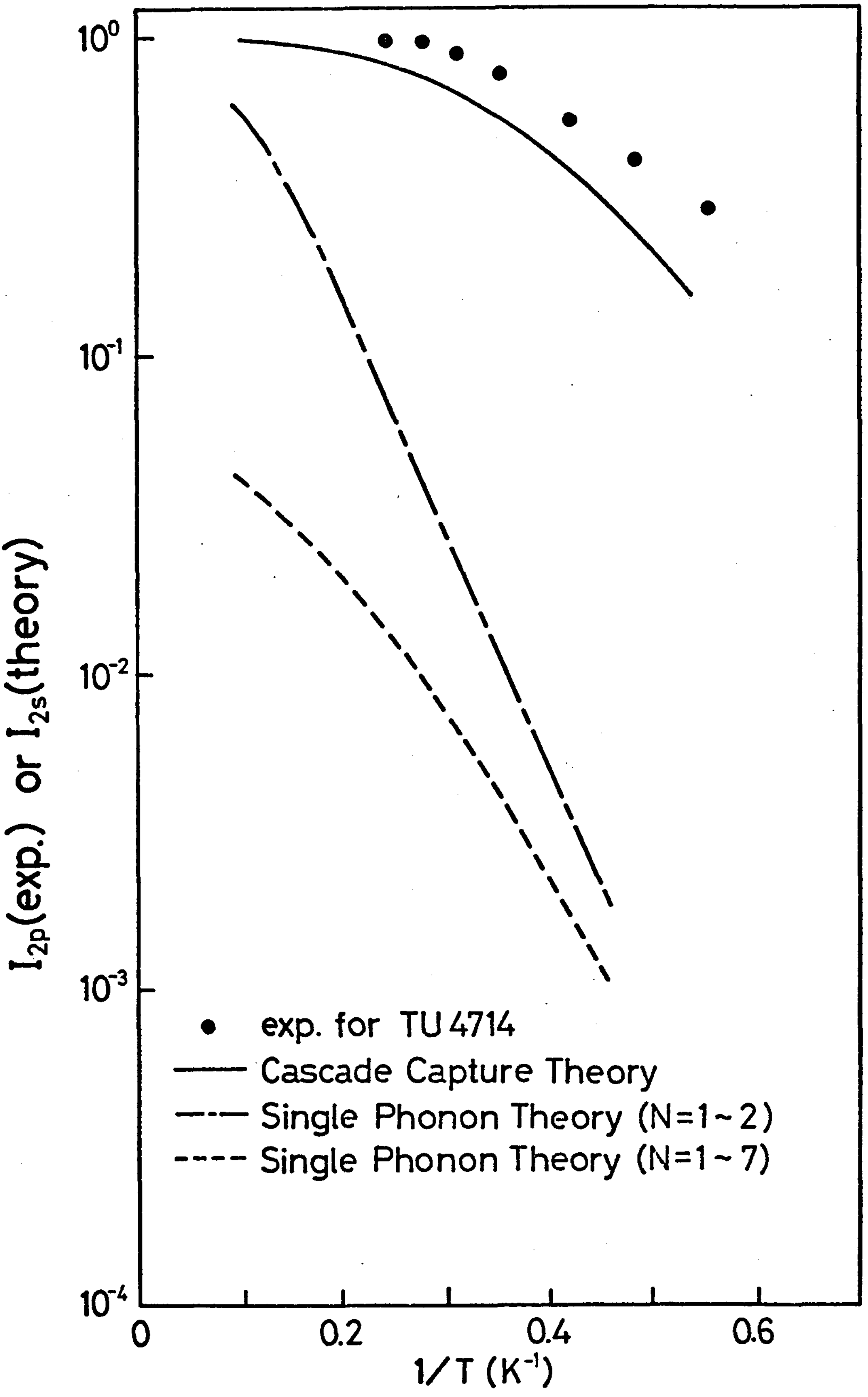

Fig.23. Theoretical temperature dependences of the thermal ionization probabilities associated with the 2s excited state; the solid curve was obtained from the cascade capture theory and the other two curves were calculated based on the assumption of single electron-phonon interactions and the participating levels of $n \leq 7$ and $n \leq 2$. Experimental result for the sample TU4714 replotted from Fig.21 (closed circles) are also shown.

Fig.24 shows the sticking probabilities for the bound states $n \leq 7$, and the sticking probabilities for the higher bound states are very small, the order of magnitude of 10^{-1} to 10^{-2}. Therefore most of the electrons transfered from the 2s excited state to the higher excited states by absorption of phonons are elevated to the conduction band.
This is the reason why the activation energy of electrons in the 2s excited state calculated by use of the cascade capture model is very small.
And in the cascade capture model, the activation energy associated with the 2s excited state increases with decreasing temperature and converges to the energy separation between the 2s excited state and the bottom of the conducdtion band, because at sufficiently low temperature multiple electron-phonon interactions can be neglected. In the experiment of the photoconductivity due to the photothermal ionization in Ge performed by Nagasaka and Narita,[11)] the activation energy associated with the 2p excited state agreed well with the energy separation between the 2p excited state and the bottom of the conduction band.
The difference of the Ge case from the GaAs one is attributed to the reason that the impurity state in Ge is deeper than that in GaAs, therefore the experimental results in Ge correspond to those in GaAs at sufficiently low temperature.

Fig.25 shows the reciprocal recombination constant (B_T^{-1}) calculated by the use of the cascade capture model (solid line), and other two theoretical curves which are calculated by a modified theory for impure samples and will be described later in detail.

The temperature change of the experimental photoconductivity must be proportional to that of the theoretical reciprocal recombination constant as shown in Eq.(4.1.8), if we neglect the temperature variation

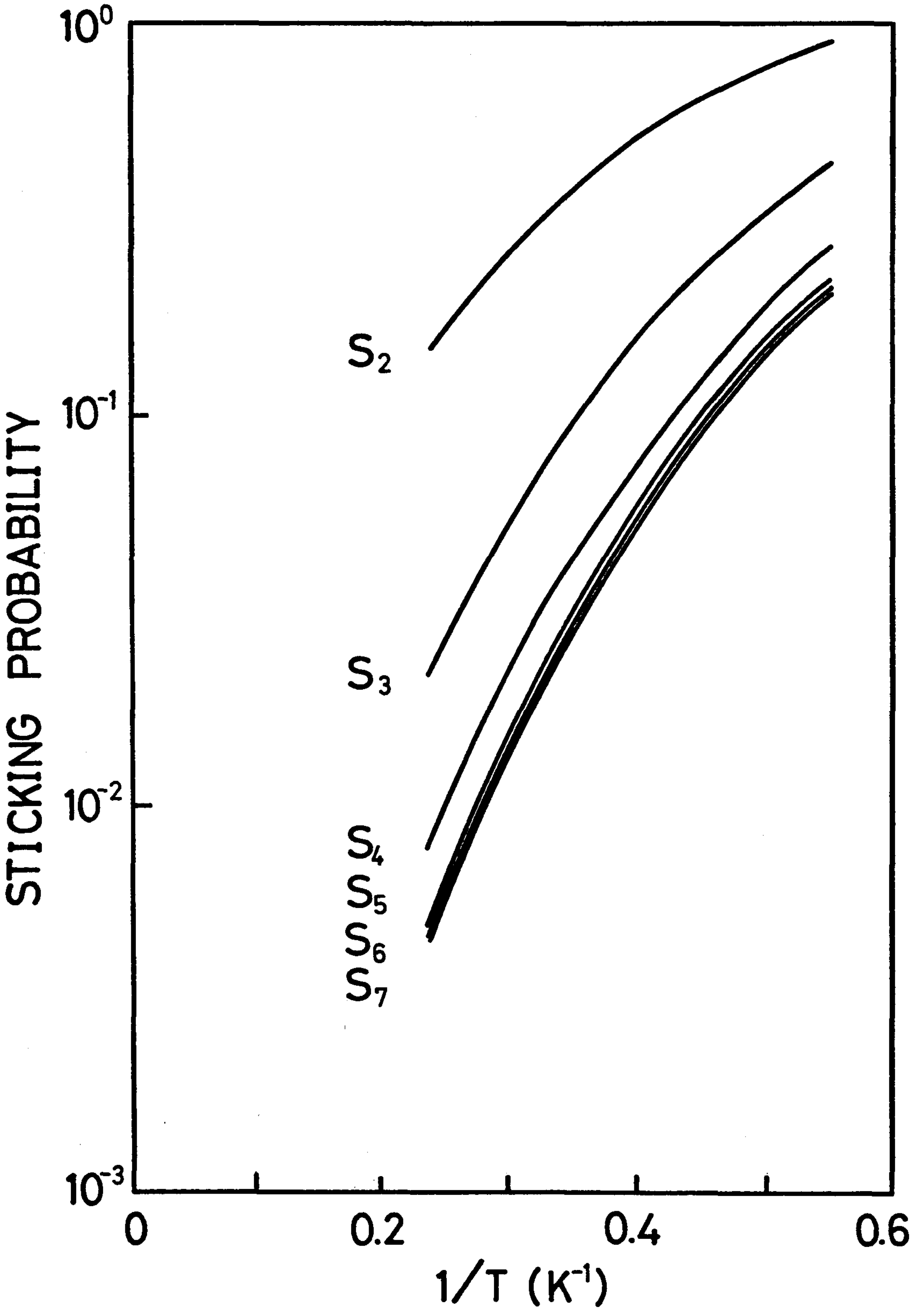

Fig.24. Theoretical temperature dependences of the sticking probabilities for the bound states $n \leq 7$ calculated from the cascade capture theory.

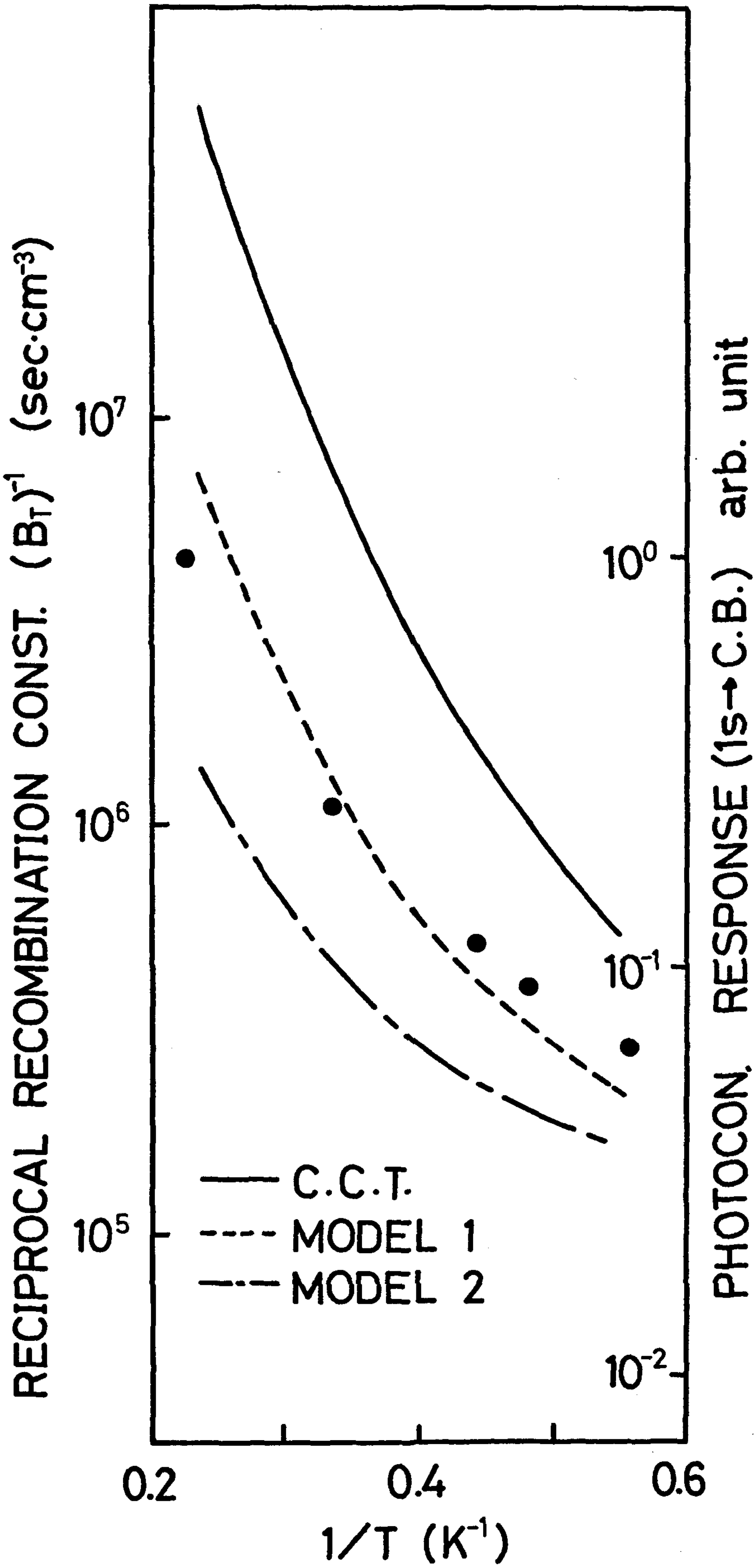

Fig.25. Theoretical temperature dependences of the reciprocal recombination constant. The solid curve is derived from the normal cascade capture theory and the other two curves are obtained from the modified theory for impure samples based on model 1 and model 2. The closed circles are the reproductions from the experimental data of the photoconductive response for TU4714 in Fig.22.

of the electron mobility in the conduction band and the impurity conduction in the excited state. In Fig.25 experimental result replotted from Fig.22 for the high purity specimen TU4714 corresponds with the calculated curve for the cascade capture theory (the solid curve shown in Fig.25), however the agreement between experiment and theory is not satisfactory. In this calculation by use of the cascade capture model, the excited donor states $n \leq 7$ are assumed to be localized ones, however, the high excited donor states must have radii overlapping each other even in currently available samples. This is the reason, we suppose, why some disagreements are observed between theoretical results and experimental ones.

(c) Modification of the cascade capture model and its application to the experimental results for doped samples

Donor concentration dependence of photoconductive response can not be explained by the theory of the simple cascade capture model proposed by A.R..[43)] All impurity states considered in the cascade capture model are assumed to be localized. However, we have no detailed knowledge about the modifications of the wave functions and density of states of the impurity levels and the conduction band due to high donor concentration. Therefore we add relative simple assumption to the above theory to explain qualitatively the experimental results due to high impurity concentration (the summarized experimental results (4) and (5)).

Assumption

With increasing donor concentration, the impurity states undergo changes from the high excited states toward the low states as the results of interactions between neighbouring donors. The assumption is that the sticking probabilities of the high excited states become larger with increasing concentration. In other words, role of the high excited states to transfer electrons from the lower states to the conduction band is reduced and that the recombination of free electrons with the high excited states become active with increasing donor concentration.

In order to express the reduction of the sticking probabilities of the high excited state in the cascade capture theory, the transition probability between states n and n', $w_{n'n}$, and the thermal ionization probability, β_n, of the high excited states are reduced in the formulation and the values of the matrix elements of electron phonon interactions involved in $w_{n'n}$ and β_n are assumed for a convenience to be reduced according to the following models 1 and 2.

model 1. (for the case of doped sample); the values of the matrix elements in $w_{n'n}$ and β_n are reduced as if the amplitudes of the wave functions for the impurity states $4 \leq n \leq 7$ and for the conduction band may be reduced by a factor of 0.3.

model 2. (for the case of highly doped sample); the values of the matrix elements in $w_{n'n}$ and β_n are reduced as if the amplitudes of the wave functions for the impurity states $5 \leq n \leq 7$ and for the conduction band may be reduced by a factor of 0.1, and for the states $3 \leq n \leq 4$ by a factor of 0.3.

In the both models 1 and 2, the wave functions for the impurity states n=1,2 are not varied. Besides the modified wave functions are used only for the calculation of the sticking probabilities of the excited states and the wave functions are assumed not to change largely in the calculation of the recombination cross-section $\sigma_c(j)$, because the density of states of the high excited states is supposed to increase with increasing the impurity concentration.

Fig.26 shows the thermal ionization probabilities associated with the 2s excited states calculated by the cascade capture model for a pure sample (replotted from Fig.23) and those by the modified model for impure samples (models 1 and 2). In the figure, it is shown that the saturation temperature at which the thermal ionization probability becomes unity increases with increasing donor concentrations. However in the calculated curve, the temperature independent photoconductivity shown in Fig.21 in the low temperature region are not appeared, because the temperature independent photoconductive response by the excitation corresponding to the energy between the ground state and 2p excited state is considered to be originated in the impurity conduction in the excited state, and this mechanism is ignored in the models 1 and 2.

Fig.25 shows the reciprocal recombination constants calculated in the cascade capture model for a pure sample and those for doped samples (model 1 and 2). The reciprocal recombination constant and its temperature change are shown to become smaller with increasing donor concentration.

The temperature independent photoconductivity for the highly doped specimen FU1215 below 3K (Fig.22) are supposed to be attributed to an impurity conduction occuring through the excited states $n \geq 2$ which is ignored in the above theory.

It has been mentioned previously in relation to Fig.21 that the electronic conduction in the 2p excited state becomes dominant in the photoconductivity due to photo-thermal ionization below 2.7K. In this case, the transition probability from the 2p excited state to the ground state by emitting a single acoustic phonon is almost independent of

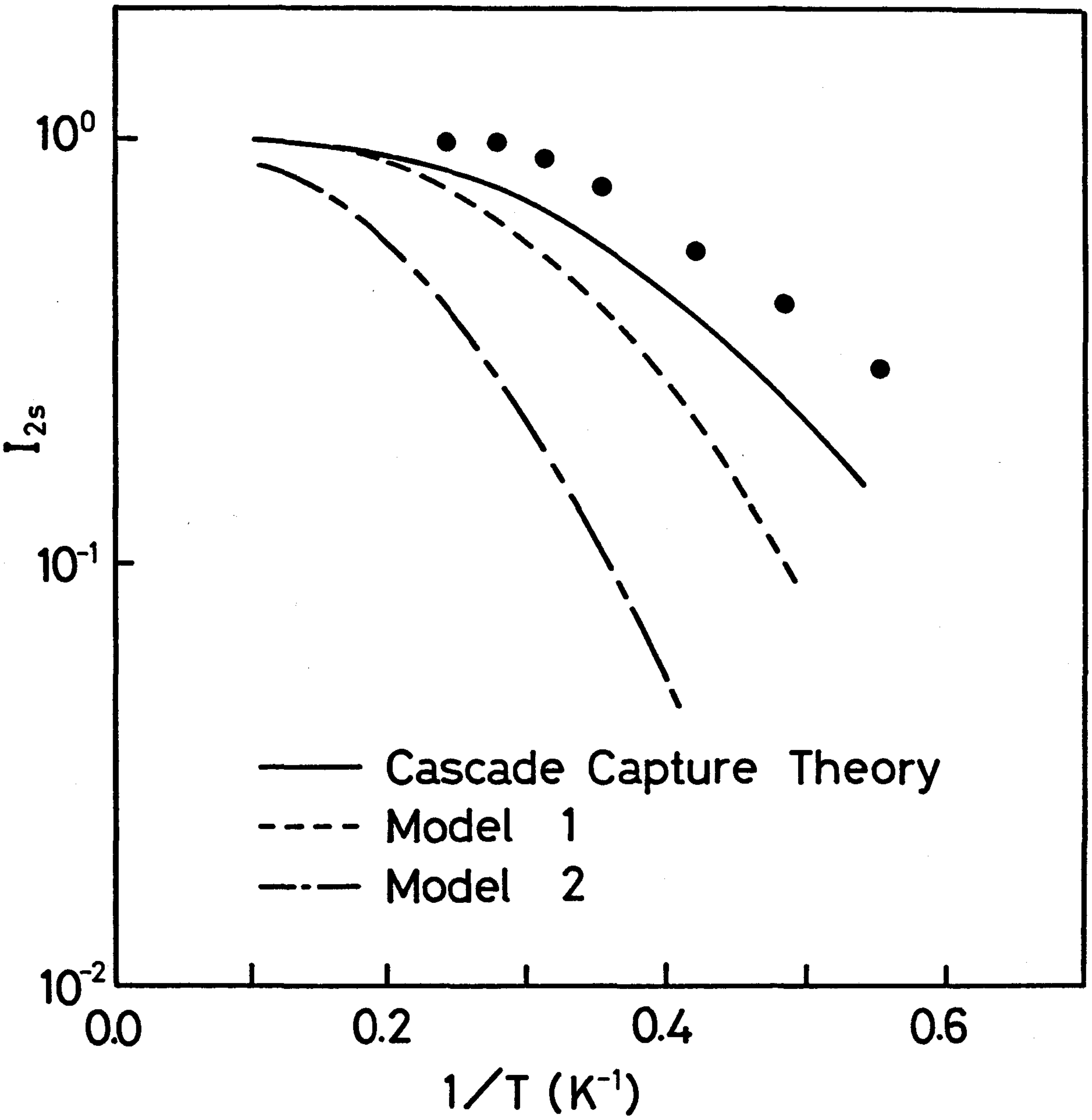

Fig.26. The theoretical temperature dependences of the thermal ionization probabilities of the electrons in the 2s excited state. The solid curve is derived from the normal cascade capture theory (replotted from Fig.23) and the other two curves are obtained from the modified theory for impure samples based on the model 1 and model 2. The closed circles are the reproductions from the experimental data for TU4714 in Fig.21.

temperature, because the energy separation between these states is about 53.4K and it is much larger than the lattice temperature of the specimen. This fact can well explain the experimental result shown in Figs.21 and 22.

Appendix A.

Energy formulae in the variational calculations

(001) state; in K.L. type wave function

$$E = \frac{5 + 3\varepsilon^2}{5\, a_\perp} + \frac{3}{4}\gamma^2 a_\perp^2 - \frac{3\varepsilon}{4 a_\perp} \cdot \left\{ \frac{-\varepsilon^2}{(1-\varepsilon^2)^{3/2}} \mathrm{Ln}(\varepsilon) + \frac{2}{1-\varepsilon^2} \right\}$$

with

$$a_\perp = -\frac{8(1-\varepsilon^2)^{5/2}}{15\,\varepsilon} \cdot \left\{ \mathrm{Ln}(\varepsilon) - \frac{2(1+2\varepsilon^2)\sqrt{1-\varepsilon^2}}{3\,\varepsilon^2} \right\}^{-1}$$

$$\gamma^2 = \frac{4(2+3\varepsilon^2)}{15\, a_\perp^4} - \frac{\varepsilon}{2 a_\perp^3} \cdot \left\{ -\frac{\varepsilon^2}{(1-\varepsilon^2)^{3/2}} \mathrm{Ln}(\varepsilon) + \frac{2}{1-\varepsilon^2} \right\}$$

(001) state; in Y.K.A. type wave function

$$E = \frac{2 + 3\varepsilon^2}{4 a_\perp^2} + \frac{1}{2}\gamma^2 a_\perp^2 - \sqrt{\frac{2}{\pi}} \cdot \frac{\varepsilon}{a_\perp} \cdot \left\{ \frac{-\varepsilon^2}{(1-\varepsilon^2)^{3/2}} \mathrm{Ln}(\varepsilon) + \frac{2}{1-\varepsilon^2} \right\}$$

with

$$a_\perp = -\sqrt{\frac{\pi}{2}} \cdot \frac{(1-\varepsilon^2)^{5/2}}{2\,\varepsilon} \cdot \left\{ \mathrm{Ln}(\varepsilon) - \frac{2(1+2\varepsilon^2)\cdot\sqrt{1-\varepsilon^2}}{3\,\varepsilon^2} \right\}^{-1}$$

$$\gamma^2 = \frac{2 + 3\varepsilon^2}{2 a_\perp^4} - \sqrt{\frac{2}{\pi}} \cdot \frac{\varepsilon}{a_\perp^3} \cdot \left\{ \frac{-\varepsilon^2}{(1-\varepsilon^2)^{3/2}} \mathrm{Ln}(\varepsilon) + \frac{2}{1-\varepsilon^2} \right\}$$

where

$$\varepsilon = a_\perp / a_\parallel$$

$$\mathrm{Ln}(\varepsilon) = \ln \frac{1 + \sqrt{1-\varepsilon^2}}{1 - \sqrt{1-\varepsilon^2}}$$

(101) state; in Y.K.A. type wave function

$$
\begin{aligned}
E = {} & \frac{2\alpha_\perp^4}{\alpha_\perp^4 a_\perp^4} \cdot \left\{ \frac{2+3\varepsilon^2}{4a_\perp^2} + \frac{\gamma^2 a_\perp^2}{2} - \sqrt{\frac{2}{\pi}} \cdot \frac{\varepsilon}{a_\perp} \cdot \left\{ \frac{-\varepsilon^2}{(1-\varepsilon^2)^{3/2}} \cdot \mathrm{Ln}(\varepsilon) \right.\right. \\
& \left.\left. + \frac{2}{1-\varepsilon^2} \right\} \right\} + \frac{\varepsilon^3 (a_\perp^2 + \alpha_\perp^2)^2}{16\pi\sqrt{2\pi}\, a_\perp^9 (a_\perp^4 + \alpha_\perp^4)} \cdot \left\{ \frac{8\pi\sqrt{2\pi}\, a_\perp^7}{\varepsilon^3} \right. \\
& + \frac{24\pi\sqrt{2\pi}\,\gamma^2 a_\perp^{11}}{\varepsilon^3} + \frac{12\pi\sqrt{2\pi}\, a_\perp^7}{\varepsilon} + \frac{192\pi a_\perp^8}{1-\varepsilon^2} \\
& \left. \cdot \left\{ -\frac{8+10\varepsilon^2-3\varepsilon^4}{24\varepsilon^2(1-\varepsilon^2)^2} + \frac{\varepsilon^4-4\varepsilon^2+8}{16(1-\varepsilon^2)^{5/2}} \cdot \mathrm{Ln}(\varepsilon) \right\} \right\} \\
& - \frac{\varepsilon^3 \alpha_\perp^2 (a_\perp^2 + \alpha_\perp^2)}{2\pi\sqrt{2\pi}\, a_\perp^7 (\alpha_\perp^4 + a_\perp^4)} \cdot \left\{ \frac{4\pi\sqrt{2\pi}\,\gamma^2 a_\perp^9}{\varepsilon^3} + \frac{3\pi\sqrt{2\pi}\, a_\perp^5}{\varepsilon} \right. \\
& \left. + \frac{32\pi a_\perp^6}{1-\varepsilon^2} \cdot \left\{ -\frac{2+\varepsilon^2}{4\varepsilon^2(1-\varepsilon^2)} + \frac{4-\varepsilon^2}{8(1-\varepsilon^2)^{3/2}} \cdot \mathrm{Ln}(\varepsilon) \right\} \right\}
\end{aligned}
$$

where $\alpha_\perp$ and $\alpha_{/\!/}$ mean the optimum values of $a_\perp$ and $a_{/\!/}$ for (001) state in the same magnetic field

(112) state; in Y.K.A. type wave function

$$E = \Big\{ 1 + \frac{3a_\perp^4}{4\varepsilon^4}\left(\frac{\varepsilon^2}{a_\perp^2}+\frac{1}{\alpha_\parallel^2}\right)^2 - \frac{a_\perp^2}{\varepsilon^2}\left(\frac{\varepsilon^2}{a_\perp^2}+\frac{1}{\alpha_\parallel^2}\right)\Big]^{-1} \cdot \Big\{ \frac{4+\varepsilon^2}{4a_\perp^2} + \gamma^2 a_\perp^2$$

$$- \frac{\varepsilon}{\sqrt{2\pi}\,a_\perp} \cdot \Big\{ \frac{2-\varepsilon^2}{(1-\varepsilon^2)^{3/2}} \cdot \mathrm{Ln}(\varepsilon) - \frac{2}{1-\varepsilon^2} \Big\}\Big\} + \frac{\varepsilon}{16\pi\sqrt{2\pi}\,a_\perp^5} \cdot \left(\frac{\varepsilon^2}{a_\perp^2}+\frac{1}{\alpha_\parallel}\right)^2$$

$$\cdot \Big\{ 1 + \frac{3a_\perp^4}{4\varepsilon^4} \cdot \left(\frac{\varepsilon^2}{a_\perp^2}+\frac{1}{\alpha_\parallel^2}\right)^2 - \frac{a_\perp^2}{\varepsilon^2}\left(\frac{\varepsilon^2}{a_\perp^2}+\frac{1}{\alpha_\parallel^2}\right)\Big]^{-1} \cdot \Big\{ \frac{12\pi\, 2\pi\, \gamma^2 a_\perp^{11}}{\varepsilon^5} + \frac{7\pi\sqrt{2\pi}\, a_\perp^7}{\varepsilon^3}$$

$$+ \frac{192\pi\, a_\perp^8}{(1-\varepsilon^2)^2} \cdot \Big\{ \frac{3\varepsilon^4 + 16\varepsilon^2 - 4}{24\varepsilon^4(1-\varepsilon^2)} + \frac{\varepsilon^2 - 6}{16(1-\varepsilon^2)^{3/2}} \cdot \mathrm{Ln}(\varepsilon) \Big\}\Big\}$$

$$- \frac{\varepsilon}{4\pi\sqrt{2\pi}\,a_\perp^5} \cdot \left(\frac{\varepsilon^2}{a_\perp^2}+\frac{1}{\alpha_\parallel^2}\right) \cdot \Big\{ 1 + \frac{3a_\perp^4}{4\varepsilon^4}\left(\frac{\varepsilon^2}{a_\perp^2}+\frac{1}{\alpha_\parallel^2}\right)^2 - \frac{a_\perp^2}{\varepsilon^2}\left(\frac{\varepsilon^2}{a_\perp^2}+\frac{1}{\alpha_\parallel^2}\right)\Big]^{-1}$$

$$\cdot \Big\{ \frac{4\pi\sqrt{2\pi}\,a_\perp^5}{\varepsilon^3} + \frac{4\pi\sqrt{2\pi}\,\gamma^2 a_\perp^9}{\varepsilon^3} - \frac{\pi\sqrt{2\pi}\,a_\perp^5}{\varepsilon} + \frac{32\pi\, a_\perp^6}{1-\varepsilon^2}$$

$$\cdot \Big\{ -\frac{\varepsilon^2+2}{4\varepsilon^2(1-\varepsilon^2)} + \frac{4-\varepsilon^2}{8(1-\varepsilon^2)^{3/2}} \cdot \mathrm{Ln}(\varepsilon) \Big\}\Big\} + \gamma$$

where $\alpha_\perp$ and $\alpha_\parallel$ mean the optimum values of $a_\perp$ and $a_\parallel$ for (110)state in the same magnetic field.

(210) state; in Y.K.A. type wave function

$$
\begin{aligned}
E = {} & \frac{8\,\alpha_\perp^4}{3a_\perp^4 - 2\,a_\perp^2\alpha_\perp^2 + 3\alpha_\perp^4} \cdot \Bigg\{ \frac{4+\varepsilon^2}{4a_\perp^2} + \gamma^2 a_\perp^2 - \frac{\varepsilon}{\sqrt{2\pi}\,a_\perp} \cdot \Bigg\{ \frac{2-\varepsilon^2}{(1-\varepsilon^2)^{3/2}} \cdot \mathrm{Ln}(\varepsilon) \\
& - \frac{2}{1-\varepsilon^2} \Bigg\}\Bigg\} + \frac{\varepsilon\,(a_\perp^2+\alpha_\perp^2)^2}{32\pi\sqrt{2\pi}\,a_\perp^9\,(3a_\perp^4 - 2a_\perp^2\alpha_\perp^2 + 3\alpha_\perp^4)} \cdot \Bigg\{ \frac{64\pi\sqrt{2\pi}\,a_\perp^7}{\varepsilon} \\
& + \frac{192\pi\sqrt{2\pi}\,\gamma^2 a_\perp^{11}}{\varepsilon} + 24\pi\sqrt{2\pi}\,\varepsilon\,a_\perp^7 - \frac{24\pi\,a_\perp^8}{\sqrt{1-\varepsilon^2}} \\
& \cdot \Bigg\{ \frac{16-24\varepsilon^2+18\varepsilon^4-5\varepsilon^6}{2\,(1-\varepsilon^2)^3} \cdot \mathrm{Ln}(\varepsilon) + \frac{-15\varepsilon^4+44\varepsilon^2-44}{3\,(1-\varepsilon^2)^{5/2}} \Bigg\}\Bigg\} \\
& - \frac{2\varepsilon\,\alpha_\perp^2\,(a_\perp^2+\alpha_\perp^2)}{4\pi\sqrt{2\pi}\,a_\perp^7\,(3a_\perp^4 - 2a_\perp^2\alpha_\perp^2 + 3\alpha_\perp^4)} \cdot \Bigg\{ \frac{8\pi\sqrt{2\pi}\,a_\perp^5}{\varepsilon} + \frac{24\pi\sqrt{2\pi}\,\gamma^2 a_\perp^9}{\varepsilon} \\
& + 4\pi\sqrt{2\pi}\,\varepsilon\,a_\perp^5 - \frac{8\pi\,a_\perp^6}{\sqrt{1-\varepsilon^2}} \cdot \Bigg\{ \frac{3\varepsilon^4-8\varepsilon^2+8}{2(1-\varepsilon^2)^2} \cdot \mathrm{Ln}(\varepsilon) + \frac{3(\varepsilon^2-2)}{(1-\varepsilon^2)^{3/2}} \Bigg\}\Bigg\} \\
& + \gamma
\end{aligned}
$$

where $\alpha_\perp$ and $\alpha_{/\!/}$ mean the optimum values of $a_\perp$ and $a_{/\!/}$ for (110) state in the same magnetic field

Appendix B.

Computer program for the variational calculations of (112) state

```
C     ZEEMAN SPILITING IN GAAS    (Y.K.A. (3P M=+1) -GAM)    B-H THEORY
      DIMENSION F(300)
      PAI=3.14159
      TPAI=SQRT(2.*PAI)
      PTEMP=PAI*TPAI
  100 CONTINUE
C     AINI=ALFA.PERP   ALFA=ALFA.PARA
      READ(2,2001) GAM,AINI,ALFA
 2001 FORMAT(3F10.5)
      GAMD=GAM*GAM
      ALFA2=ALFA*ALFA
      EP=0.57
  200 CONTINUE
      EPD=EP*EP
      EP3=EP*EPD
      EP4=EPD*EPD
      EP5=EP*EP4
      TEMP=1.-EPD
      TEMP1=SQRT(TEMP)
      TEMP3=TEMP1**3
C     AN=LN
      AN=ALOG((1.+TEMP1)/(1.-TEMP1))
      APERP=AINI
      DO 300 I=1,200
      APERP2=APERP*APERP
      APERP4=APERP2*APERP2
      APERP5=APERP4*APERP
      APERP6=APERP4*APERP2
```

```
      APERP7=APERP6*APERP
      APERP8=APERP6*APERP2
      APERP9=APERP7*APERP2
C     Y=11.
      APERPY=APERP9*APERP2
      FTEMP1=EPD/APERP2+1./ALFA2
      FTEMP2=1./(1.+3.*APERP4/(4.*EP4)*FTEMP1*FTEMP1-APERP2/EPD*FTEMP1)
      FTEMP3=3.*EP4+16.*EPD-4.
      F1=FTEMP2*((4.+EPD)/(4.*APERP2)+GAMD*APERP2
     1-EP/(TPAI*APERP)*((2.-EPD)/TEMP3*AN-2./TEMP))
      F2=EP/(16.*PTEMP*APERP5)*FTEMP1*FTEMP1*FTEMP2
     1*(12.*PTEMP*APERP7/EP5+12.*PTEMP*GAMD*APERPY/EP5
     2+7.*PTEMP*APERP7/EP3+192.*PAI*APERP8/(TEMP*TEMP)
     3*(FTEMP3/(24.*EP4*TEMP)+(EPD-6.)/(16.*TEMP3)*AN))
      F3=EP/(4.*PTEMP*APERP5)*FTEMP1*FTEMP2
     1*(4.*PTEMP*APERP5/EP3+4.*PTEMP*GAMD*APERP9/EP3
     2-PTEMP*APERP5/EP+32.*PAI*APERP6/TEMP
     3*((-EPD-2.)/(4.*EPD*TEMP)+(4.-EPD)/(8.*TEMP3)*AN))
      ENER=F1+F2-F3
      F(I)=ENER
      APERP=APERP+0.01
  300 CONTINUE
      WRITE(3,3001) EP,GAM,AINI,ALFA
 3001 FORMAT(1H ,3HEPS,9X,3HGAM,8X,2HA0,9X,2HAP/1H ,4E11.4)
      WRITE(3,3002) (F(I),I=1,200)
 3002 FORMAT(1H ,4HENER/10E11.4)
      EP=EP-0.01
      IF(EP.GT.0.45) GO TO 200
      GO TO 100
      END
```

Appendix C.

Computer program for the normal cascade capture calculation

```
C     EI=RY     N=1--7
C     RECOMBINATION CF GAAS (A-R) (COULOMB FUNC. FOR C-B)  M.MIYAO
      COMMON NBS,IJK,T,H,CS,A,XK,EI,EN
      EXTERNAL FUNC
      DIMENSION T(10),BETAN(7),SIGCN(7),OMENN(7.7).SOME(7).PNN(7.7).
     *PMMEW(7),PSUM(7),SN(7),PNNEW(7)
      READ(5,100)(T(IJK),IJK=1,10)
  100 FORMAT(10F6.3)
      MEW=3.*10.**4
      E1=1.42*10.0**(-11)
      H=1.05*10.0**(-27)
      CS=1.88*10.**(5)
      R=5.31
      A=9.8*10.0**(-7)
      EI=9.38*10.0**(-15)
      RY=9.38*10.0**(-15)
      XM=0.61*10.0**(-28)
      XK=1.38*10.0**(-16)
      IJK=1
    1 TEMP3=64.*E1**2*H**4*CS**3/(3.14*R*A**8*RY**5)
      DO 111 NBS=1,7
      XNBS=FLOAT(NBS)
      TEMP1=8.*E1**2*H*CS**3*XNBS**7/(R*A**5*RY**5)
      TEMP4=(2.*XM*XK*T(IJK)/3.14)**1.5
      EN=(1.-1./(XNBS**2))*RY
      TEMP5=EXP(-(EI-EN)/(XK*T(IJK)))
      TEMP11=256.*E1**2*XM*H**2*CS**3/(3.14*R*A**6*XNBS**3*XK**4
     **T(IJK)**4)
      HH=EI/(XK*T(IJK))
      D2=(XK*T(IJK))/(EI-FN)
      D1=D2/101.
      DI=10**(-40)
      L=100
      CALL SINT1(D1,C2,DI,AIG.D,L,FUNC,INDFR)
      BETAN(NBS)=TEMP11*AIG
      TEMP2=2.*3.14**2*H**3/(2.*XM*XK**2*T(IJK)**2)
      TEMP6=EXP((EI-EN)/(XK*T(IJK)))
```

```
  111 SIGCN(NBS)=TEMP2*BETAN(NBS)*TEMP6
      DO 1600 NK=2,7
      DO 1700 ND=1,7
      XNK=FLOAT(NK)
      XND=FLOAT(ND)
      IF(NK-ND) 300,500,400
  300 ENDU=(1.-1./(XND**2))*RY
      EN=(1.-1./(XNK**2))*RY
      TEMP7=(XND*XNK)**5/((XNK-XND)**5*(XNK+XND)**3)
      TEMP8=1./(1.-EXP(-(EN-ENDU)/(XK*T(IJK))))
      OMENN(ND,1)=0
      OMENN(ND,NK)=TEMP3*TEMP7*TEMP8
      GO TO 1700
  400 TEMP9=(XND*XNK)**5/((XND-XNK)**5*(XNK+XND)**3)
      ENDU=(1.-1./(XND**2))*RY
      EN=(1.-1./(XNK**2))*RY
      TEMP10=1./(EXP((ENDU-EN)/(XK*T(IJK)))-1.)
      OMENN(ND,1)=0
      OMENN(ND,NK)=TEMP3*TEMP9*TEMP10
      GO TO 1700
  500 OMENN(ND,NK)=0
 1700 CONTINUE
 1600 CONTINUE
      DO 650 NK=1,7
      SOME(NK)=0
      DO 600 ND=1,7
      SOME(NK)=SOME(NK)+OMENN(ND,NK)
  600 CONTINUE
  650 CONTINUE
      DO 750 NK=1,7
      DO 700 ND=1,7
      PNN(ND,NK)=OMENN(ND,NK)/(BETAN(NK)+SOME(NK))
  700 CONTINUE
  750 CONTINUE
      DO 800 NK=2,7
  800 PNNEW(NK)=BETAN(NK)/(BETAN(NK)+SOME(NK))
      PNNEW(1)=0
      WRITE(6,1632) IJK
 1632 FORMAT(1H1,6HNUMBER,I3)
      INE=1
```

```
      DO 10 I=1,7
   10 PSUM(I)=0
 1118 DO 1100 NK=2,7
      PMMEW(NK)=0
      DO 1200 ND=1,7
      PMMEW(NK)=PMMEW(NK)+PNN(ND,NK)*PNNEW(ND)
      PMMEW(1)=0
 1200 CONTINUE
 1100 CONTINUE
      DO 1300 NK=1,7
 1300 PSUM(NK)=PSUM(NK)+PNNEW(NK)
      IF(INE .LT. 1000) GO TO 1555
      IF(INE .GT. 10000) GO TO 1553
      IMOE=MOD(INE,1000)
      GO TO 1554
 1553 IMOE=MOD(INE,10000)
 1554 IF(IMOE) 1555,1551,1555
 1551 WRITE(6,1631) INE,(PNNEW(I),I=1,7)
 1631 FORMAT(6H MEW=,I6/5X.9HPNNEW(7)=,7E13.4)
      DO 1663 I=1,7
 1663 SN(I)=1.-PSUM(I)
      SIGM=0.
      DO 1665 I=1,7
 1665 SIGM=SIGM+SIGCN(I)*SN(I)
      WRITE(6,1634)(SN(I),I=1,7),SIGM
 1634 FORMAT(7H SN(7)=,7E13.4.10X,5HSIGM=,E13.4)
 1555 DO 20 I=1,7
   20 PNNEW(I)=PMMEW(I)
      INE=INE+1
      IF(INE-MEW) 1118,1118,1119
 1119 DO 1400 NK=1,7
 1400 SN(NK)=1-PSUM(NK)
      SIGM=0
      DO 1500 NK=1,7
 1500 SIGM=SIGM+SIGCN(NK)*SN(NK)
      WRITE(6,1710) IJK,T(IJK)
 1710 FORMAT(1H0,6HNUMBER,I3,5X,3HT =,F6.2)
```

```
      WRITE(6,1711)
 1711 FORMAT(10X,24H N = 1, 2, 3, 4, 5, 6, 7)
      WRITE(6,1712) (BETAN(I),I=1,7),(SIGCN(I),I=1,7),(SN(I),I=1,7),SIGM
 1712 FORMAT(6H BETAN,7E13.4/8H SIGMACN,7E13.4/4H FSN,7E13.4/6H SIGMA,
     1E13.4/14H  OMEGANN(7,7))
      DO 1714 I=1,7
 1714 WRITE(6,1713) (OMENN(I,J),J=1,7)
 1713 FORMAT(5X,7E13.4)
      WRITE(6,1723)
 1723 FORMAT(12H   PNN(7,7)=)
      DO 1722 I=1,7
 1722 WRITE(6,1721)(PNN(I,J),J=1,7)
 1721 FORMAT(5X,7E13.4)
      IJK=IJK+1
      IF(IJK-10) 1,1,1210
 1210 STOP
      END
```

```
      FUNCTION FUNC(X)
      COMMON NBS,IJK,T,H,CS,A,XK,EI,EN
      DIMENSION T(10)
      G=2*H*CS/(A*XK*T(IJK))
      XNBS=FLOAT(NBS)
      FUNC=X**3*EXP(-1*X**(-1)-(G**2/XNBS)*X**2)
      RETURN
      END
```

Appendix D.

The thermal ionization probability, β_n (written as BETAN), the capture cross section, $\sigma_c(n)$ (written as SIGMACN)and the transition probability between states n and n', $w_{n'n}$ (written as OMEGANN) obtained from the calculation by the normal cascade capture theory.

NUMBER 1 T = 9.99

n	1	2	3	4	5	6	7
BETAN	.1957E+02	.1937E+06	.4500E+07	.2740E+08	.9432E+08	.2341E+09	.4645E+09
SIGMACN	.1737E-17	.1045E-15	.9434E-15	.4127E-14	.1219E-13	.2784E-13	.5254E-13

OMEGANN(7,7)

n' \ n	2	3	4	5	6	7
1	.1207E+06	.1203E+05	.3417E+04	.1432E+04	.7351E+03	.4277E+03
2	.0	.1030E+08	.6656E+06	.1597E+06	.6161E+05	.3023E+05
3	.4002E+07	.0	.2607E+09	.1223E+08	.2494E+07	.8764E+06
4	.1858E+06	.1873E+09	.0	.3129E+10	.1197E+09	.2162E+08
5	.3825E+05	.7537E+07	.2685E+10	.0	.2315E+11	.7702E+09
6	.1358E+05	.1415E+07	.9449E+08	.2130E+11	.0	.1231E+12
7	.6338E+04	.4728E+06	.1624E+08	.6740E+09	.1171E+12	.0

NUMBER 2 T = 6.67

n	1	2	3	4	5	6	7
BETAN	.5076E+00	.7191E+05	.2835E+07	.2096E+08	.7914E+08	.2067E+09	.4230E+09
SIGMACN	.2988E-17	.2029E-15	.1942E-14	.8751E-14	.2627E-13	.6058E-13	.1150E-12

OMEGANN(7,7)

n' \ n	2	3	4	5	6	7
1	.1200E+06	.1201E+05	.3412E+04	.1430E+04	.7341E+03	.4272E+03
2	.0	.8314E+07	.5630E+06	.1376E+06	.5359E+05	.2644E+05
3	.2019E+07	.0	.1879E+09	.9098E+07	.1886E+07	.6691E+06
4	.8331E+05	.1145E+09	.0	.2168E+10	.8449E+08	.1544E+08
5	.1619E+05	.4408E+07	.1724E+10	.0	.1578E+11	.5311E+09
6	.5567E+04	.8068E+06	.5931E+08	.1393E+11	.0	.8320E+11
7	.2547E+04	.2655E+06	.1005E+08	.4349E+09	.7718E+11	.0

NUMBER 3 T = 5.00

n	1	2	3	4	5	6	7
BETAN	.1370E-01	.2713E+05	.1797E+07	.1608E+08	.6650E+08	.1826E+09	.3854E+09
SIGMACN	.4315E-17	.3190E-15	.3198E-14	.1478E-13	.4501E-13	.1047E-12	.1999E-12

OMEGANN(7,7)

n' \ n	2	3	4	5	6	7
1	.1199E+06	.1201E+05	.3411E+04	.1430E+04	.7341E+03	.4272E+03
2	.0	.7418E+07	.5204E+06	.1288E+06	.5049E+05	.2499E+05
3	.1123E+07	.0	.1518E+09	.7569E+07	.1592E+07	.5696E+06
4	.4068E+05	.7840E+08	.0	.1686E+10	.6692E+08	.1236E+08
5	.7416E+04	.2879E+07	.1241E+10	.0	.1207E+11	.4111E+09
6	.2462E+04	.5129E+06	.4174E+08	.1022E+11	.0	.6314E+11
7	.1102E+04	.1660E+06	.6973E+07	.3149E+09	.5712E+11	.0

NUMBER 4 T = 4.20

n	1	2	3	4	5	6	7
BETAN	.8999E-03	.1306E+05	.1276E+07	.1317E+08	.5832E+08	.1663E+09	.3592E+09
SIGMACN	.5351E-17	.4157E-15	.4293E-14	.2017E-13	.6206E-13	.1452E-12	.2784E-12

OMEGANN(7,7)

n' \ n	2	3	4	5	6	7
1	.1199E+06	.1201E+05	.3411E+04	.1430E+04	.7341E+03	.4272E+03
2	.0	.7038E+07	.5040E+06	.1256E+06	.4938E+05	.2449E+05
3	.7435E+06	.0	.1348E+09	.6861E+07	.1458E+07	.5244E+06
4	.2424E+05	.6137E+08	.0	.1455E+10	.5857E+08	.1090E+08
5	.4198E+04	.2170E+07	.1011E+10	.0	.1029E+11	.3537E+09
6	.1354E+04	.3784E+06	.3339E+08	.8447E+10	.0	.5354E+11
7	.5960E+03	.1208E+06	.5516E+07	.2576E+09	.4752E+11	.0

NUMBER 5 T = 3.33

n	1	2	3	4	5	6	7
BETAN	.1090E-04	.4015E+04	.7353E+06	.9546E+07	.4718E+08	.1430E+09	.3206E+09
SIGMACN	.7074E-17	.5852E-15	.6293E-14	.3029E-13	.9458E-13	.2234E-12	.4308E-12

OMEGANN(7,7)

n' \ n	2	3	4	5	6	7
1	.1199E+06	.1201E+05	.3411E+04	.1430E+04	.7341E+03	.4272E+03
2	.0	.6688E+07	.4904E+06	.1231E+06	.4855E+05	.2411E+05
3	.3927E+06	.0	.1167E+09	.6125E+07	.1320E+07	.4788E+06
4	.1068E+05	.4325E+08	.0	.1206E+10	.4959E+08	.9340E+07
5	.1693E+04	.1434E+07	.7620E+09	.0	.8367E+10	.2916E+09
6	.5203E+03	.2410E+06	.2441E+08	.6520E+10	.0	.4310E+11
7	.2223E+03	.7517E+05	.3956E+07	.1955E+09	.3708E+11	.0

NUMBER 6 T = 2.86

n	1	2	3	4	5	6	7
BETAN	.3359E-06	.1592E+04	.4771E+06	.7416E+07	.3994E+08	.1270E+09	.2931E+09
SIGMACN	.8458E-17	.7275E-15	.8037E-14	.3934E-13	.1241E-12	.2952E-12	.5718E-12

OMEGANN(7,7)

n′ \ n	2	3	4	5	6	7
1	.1199E+06	.1201E+05	.3411E+04	.1430E+04	.7341E+03	.4272E+03
2	.0	.6536E+07	.4854E+06	.1222E+06	.4827E+05	.2399E+05
3	.2409E+06	.0	.1072E+09	.5751E+07	.1252E+07	.4565E+06
4	.5634E+04	.3375E+08	.0	.1072E+10	.4481E+08	.8516E+07
5	.8312E+03	.1061E+07	.6283E+09	.0	.7328E+10	.2582E+09
6	.2455E+03	.1728E+06	.1964E+08	.5481E+10	.0	.3747E+11
7	.1024E+03	.5287E+05	.3132E+07	.1621E+09	.3145E+11	.0

NUMBER 7 T = 2.50

n	1	2	3	4	5	6	7
BETAN	.9785E-08	.6240E+03	.3081E+06	.5744E+07	.3375E+08	.1126E+09	.2676E+09
SIGMACN	.9881E-17	.8782E-15	.9935E-14	.4939E-13	.1574E-12	.3767E-12	.7328E-12

OMEGANN(7,7)

n′ \ n	2	3	4	5	6	7
1	.1199E+06	.1201E+05	.3411E+04	.1430E+04	.7341E+03	.4272E+03
2	.0	.6442E+07	.4827E+06	.1218E+06	.4814E+05	.2394E+05
3	.1476E+06	.0	.1001E+09	.5483E+07	.1204E+07	.4410E+06
4	.2949E+04	.2670E+08	.0	.9707E+09	.4121E+08	.7900E+07
5	.4037E+03	.7932E+06	.5265E+09	.0	.6534E+10	.2327E+09
6	.1144E+03	.1250E+06	.1603E+08	.4687E+10	.0	.3315E+11
7	.4657E+02	.3745E+05	.2515E+07	.1366E+09	.2713E+11	.0

NUMBER 8 T = 2.22

n	1	2	3	4	5	6	7
BETAN	.2864E-09	.2457E+03	.1995E+06	.4456E+07	.2854E+08	.9991E+08	.2445E+09
SIGMACN	.1132E-16	.1034E-14	.1194E-13	.6020E-13	.1936E-12	.4662E-12	.9105E-12

OMEGANN(7,7)

n′ \ n	2	3	4	5	6	7
1	.1199E+06	.1201E+05	.3411E+04	.1430E+04	.7341E+03	.4272E+03
2	.0	.6386E+07	.4813E+06	.1216E+06	.4808E+05	.2391E+05
3	.9087E+05	.0	.9481E+08	.5290E+07	.1171E+07	.4304E+06
4	.1546E+04	.2140E+08	.0	.8922E+09	.3846E+08	.7433E+07
5	.1961E+03	.5996E+06	.4480E+09	.0	.5918E+10	.2131E+09
6	.5334E+02	.9127E+05	.1328E+08	.4071E+10	.0	.2980E+11
7	.2117E+02	.2678E+05	.2049E+07	.1169E+09	.2378E+11	.0

NUMBER 9 T = 2.00

n	1	2	3	4	5	6	7
BETAN	.9012E-11	.9891E+02	.1306E+06	.3478E+07	.2423E+08	.8889E+08	.2238E+09
SIGMACN	.1273E-16	.1190E-14	.1400E-13	.7147E-13	.2318E-12	.5612E-12	.1100E-11

OMEGANN(7,7)

n' \ n	2	3	4	5	6	7
1	.1199E+06	.1201E+05	.3411E+04	.1430E+04	.7341E+03	.4272E+03
2	.0	.6351E+07	.4805E+06	.1215E+06	.4805E+05	.2390E+05
3	.5661E+05	.0	.9081E+08	.5149E+07	.1147E+07	.4230E+06
4	.8209E+03	.1740E+08	.0	.8310E+09	.3635E+08	.7077E+07
5	.9662E+02	.4594E+06	.3868E+09	.0	.5435E+10	.1977E+09
6	.2522E+02	.6754E+05	.1117E+08	.3588E+10	.0	.2717E+11
7	.9765E+01	.1939E+05	.1693E+07	.1016E+09	.2115E+11	.0

NUMBER 10 T = 1.82

n	1	2	3	4	5	6	7
BETAN	.2877E-12	.4007E+02	.8576E+05	.2721E+07	.2060E+08	.7916E+08	.2050E+09
SIGMACN	.1415E-16	.1349E-14	.1613E-13	.8328E-13	.2722E-12	.6626E-12	.1303E=11

OMEGANN(7,7)

n' \ n	2	3	4	5	6	7
1	.1199E+06	.1201E+05	.3411E+04	.1430E+04	.7341E+03	.4272E+03
2	.0	.6330E+07	.4802E+06	.1215E+06	.4804E+05	.2389E+05
3	.3538E+05	.0	.8768E+08	.5044E+07	.1130E+07	.4177E+06
4	.4367E+03	.1427E+08	.0	.7814E+09	.3465E+08	.6795E+07
5	.4768E+02	.3543E+06	.3373E+09	.0	.5041E+10	.1852E+09
6	.1195E+02	.5027E+05	.9475E+07	.3194E+10	.0	.2502E+11
7	.4513E+01	.1412E+05	.1411E+07	.8911E+08	.1900E+11	.0

T; the temperature in Kelvin,

E+08; 10^8 etc.

References

1) H.Fritzshe: J.Phys.Chem.Solids 6 69 (1959)

2) R.K.Ray and H.Y.Fan: Phys.Rev. 121 768 (1961)

3) R.J.Sladek: J.Phys.Chem.Solids 5 157 (1958)

4) H.Miyazawa and K.Ikoma: J.Phys.Soc.Japan 23 290 (1967)

5) J.H.Reuszer and P.Fisher: Phys.Rev. 165 369 (1964)

6) Y.Nisida and K.Horii: J.Phys.Soc.Japan 26 388 (1969)

7) K.Horii and Y.Nisida: J.Phys.Soc.Japan 31 783 (1971)

8) K.Colbow: Can.J.Phys. 41 1801 (1963)

9) Y.Oka and S.Narita: J.Phys.Soc.Japan 28 674 (1970)

10) T.M.Lifshitz, N.P.Lichtman and V.I.Sidorov: *Proc.Intern.Conf.Phys. Semicond.* (Moscow, 1968) p.1081

11) K.Nagasaka and S.Narita: J.Phys.Soc.Japan 35 788 (1973)

12) R.Kaplan: *Proc.Intern.Conf.Phys.Semicond.* (Kyoto, 1966) J.Phys.Soc. Japan 21 (1966) Suppl. p.249

13) J.Yamamoto, H.Yoshinaga and S.Kon: Japan.J.appl.Phys. 8 242 (1969)

14) J.R.Knight, D.Effer, and P.R.Evans: Solid State Electron. 8 178 (1965)

15) I.Akasaki and T.Hara: *Proc.Intern.Conf.Phys.Semicond.* (Moscow, 1968) p.787

16) S.Asai, T.Toyabe and M.Hirao: *Proc.Intern.Conf.Phys.Semicond.* (Boston, 1970) p.578

17) G.E.Stillman, C.M.Wolfe, J.E.Melngailis, C.D.Parker, P.E.Tannenwald and J.O.Dimmock: Appl.Phys.Lett. 13 83 (1968)

18) R.Kaplan, M.A.Kinch and W.C.Scott: Solid State Commun. 7 883 (1969)

19) G.E.Stillman, C.M.Wolfe, and J.O.Dimmock: Solid State Commun. 7 921 (1969)

20) S.Narita and M.Miyao: Solid State Commun. 9 2161 (1971)

21) H.R.Fetterman, D.M.Larsen, G.E.Stillman, P.E.Tannenwald and J.Waldman: Phys.Rev.Lett. 26 975 (1971)

22) G.E.Stillman, D.M.Larsen and C.M.Wolfe: Phys.Rev.Lett. 27 989 (1971)

23) C.M.Summers and R.Dingle: Phys.Rev.B1 1603 (1970)

24) G.E.Stillman, C.M.Wolfe and J.O.Dimmock: *Proc.3rd.Intern.Conf.Photoconductivity,* Edited by E.M.Pell (Pergamon Press 1971) p.265

25) L.J.van der Paw: Philips Res.Rep. 13 1 (1958)

26) C.M.Wolfe, G.E.Stillman and J.O.Dimmock: J.appl.Phys. 41 504 (1970)

27) Y.Yafet, R.W.Keyes, and E.N.Adams: J.Phys.Chem.Solids 1 137 (1956)

28) W.H.Kleiner: Lincoln Labs.Prog.Rept. (Feb.1958)

29) R.J.Elliott and R.Loudon: J.Phys.Chem.Solids 15 196 (1960)

30) Y.Nisida and K.Horii: J.Phys.Soc.Japan 31 776 (1971)

31) D.M.Larsen: J.Phys.Chem.Solids 29 271 (1968)

32) W.Kohn and J.M.Luttinger: Phys.Rev. 98 915 (1955)

33) R.F.Wallis and H.J.Bowlden: J.Phys.Chem.Solids 7 78 (1958)

34) W.S.Boyle and R.E.Howard: J.Phys.Chem.Solids 19 181 (1961)

35) E.H.Putley: Phys.stat.sol. 6 571 (1964)

36) N.I.Astafev, M.I.Barnik and B.I.Beglov: Soviet Physics-Semicond. 4 1240 (1971)

37) S.D.Seccombe and D.M.Korn: Solid State Commun. 11 1539 (1972)

38) G.E.Stillman, C.M.Wolfe and D.M.Korn: *Proc.Intern.Conf.Phys.Semicond.* (Warsaw, 1972) p.863

39) H.Nishimura: Phys.Rev. 138 A815 (1965)

40) W.Baltensperger: Phil.Mag. 44 1355 (1953)

41) E.M.Conwell: Phys.Rev. 103 51 (1956)

42) T.Toyabe and S.Asai: Phys.Rev. 8 1531 (1973)

43) G.Ascarelli and S.Rodriguez: Phys.Rev. 124 1321 (1961)

44) G.Ascarelli and S.C.Brown: Phys.Rev. 120 1615 (1960)

45) M.Lax: Phys.Rev. 119 1502 (1960)

46) F.Beleznay and G.Pataki: Phys.Status Solidi 13 499 (1966)

47) R.A.Brown and S.Rodriguez: Phys.Rev. 153 890 (1967)